Mineralogy and petrology of the manganese deposit at the Aosta Valley (Italy)

Nina-Maria Berghofer, BSc.

Master Thesis

Thesis submitted to the Department of applied geosciences and geophysics
at the University of Leoben, Chair for mineralogy of raw materials
in partial fulfillment of the requirements for the degree of

DIPLOMINGENIEUR

Examiner: Ao. Univ.-Prof. Dr. Ronald Bakker
Leoben, May 2011

I declare in lieu of oath, that I wrote this thesis

and performed the associated research myself,

using only literature cited in this volume.

Nina-Maria Berghofer

Leoben, May 2011

ACKNOWLEDGMENT

At this point I want to thank those people who supported me during the last years of my studies. Especially I want to thank Prof. Ronald Bakker for his great support during my studies for this thesis, for the correction and his patience.

I also want to thank Prof. Eero Hanski for his support during the scanning electron microprobe analysis in Finland. At this point, I want to give Mr. Mühlhans props for the sample preparations and his great help at the microprobe.

Last but not least I want to thank my lovely parents for their great support, their financial aid and their reassure for accomplishing my dreams. I also have to say thank you to Mr. Pura for his escort at the long and woebegone way from the beginning to the finishing of this thesis.

ABSTRACT

The deposits Prabornaz and Servette (Aosta valley, NW Italy) are located within the Zermatt-Saas-zone, which is a part of the ophiolithic Piemont zone. Prabornaz is the biggest known manganese deposit of the western Alps. The enrichment of manganese occurred by the sea floor spreading of the penninic ocean, which started in the middle Jurassic and proceeded until the early Cretaceous. From this point the deposit shared the whole high pressure metamorphism of the alpine orogeny. During the metamorphism a plurality of different manganese minerals were formed (piemontite, spessartine, braunite, macfallite, calderite, greenovite, manganoan calcite). The focus of this thesis is the mineralogy and petrology of the metamorphic rock, which have been studied with the aid of optical microscopy, Raman spectroscopy, scanning electron microscopy and microprobe. Fluid inclusions in quartz, garnet and epidote have been studied with microthermometry and Raman spectroscopy. The manganese rich minerals are analyzed with chemical methods and their forming circumstances are defined by density and composition of fluid phases in their inclusions. The fluid phase in manganese rich lithologies is H_2O-rich with minor amounts of CO_2 and N_2, and a salinity at an average of 6.17 equivalent mass% NaCl. The density is about 0.9138 g/cm^3. In contrast, the adjacent HP-metamorphic manganese-poor rocks contain highly saline fluids, with up to 19.95 equivalent mass% NaCl.

ZUSAMMENFASSUNG

Die Lagerstätten Prabornaz und Servette (Aostatal, NW-Italien) befinden sich in der Zermatt-Saas-Zone die wiederum einen Teil der ophilitischen Piemont Einheit bildet. Prabornaz ist die größte bekannte Mangan-Lagerstätte der Westalpen. Die Mangan Anreicherungen fanden während der Öffnung des penninischen Ozeans statt, die in der mittleren Jura angefangen hat und bis in die frühe Kreide dauerte. Anschließend hat die Lagerstätte die Hochdruck Metamorphose der alpinen Orogenese durchgemacht, wodurch es zu der Bildung einer Vielzahl von verschiedenstes Manganmineralen kam (Piemontit, Spessartin, Braunit, Macfallite, Calderit, Greenovit, manganreicher Kalzit). Das Augenmerk dieser Arbeit lag auf der Mineralogie und Petrologie der metamorphen Gesteine, die mit Hilfe der optischen Mikroskopie, Raman Spektroskopie, Rasterelektronenmikroskop und Elektronenmikrosonde untersucht wurden. Flüssigkeitseinschlüsse in Quarzen, Granaten und Epidote wurden mit der Mikrothermometrie und der Raman Spektroskopie analysiert. Die manganreichen Minerale sind chemisch analysiert und ihre Bildungsumstände sind durch die Dichte und die Zusammensetzung der fluiden Phasen in Einschlüssen definiert. Die fluiden Phasen in manganreichen Lithologien sind H_2O reich mit geringen Anteilen an CO_2 und N_2, die die flüssigen Phasen haben eine durchschnittliche Salinität von 6.1%, dies entspricht der Menge an NaCl die gelöst ist. Die Dichte ist um 0.9138 g/cm^3. Im Unterschied dazu, weißen die angrenzenden HP-metamorphen manganarmen Gesteine, extrem hoch salinare Flüssigkeitseinschlüsse, deren NaCl Gehalt bis durchschnittlich 19.95% reicht.

INDEX

LIST OF FIGURES

LIST OF TABLES

LIST OF DIAGRAMS

1. Geological Setting

The manganese deposit Prabornaz is located in the St. Marcel Valley. The St. Marcel Valley is a side valley in the south of the Aosta Valley (see figure 1-1). The Aosta Valley is an Alpine Valley which is located in the northwest of Italy and it includes the Italian slopes of Monte Bianco, Monte Rosa and the Matterhorn, its highest peak is Monte Bianco (4810m).

Figure 1-1: Topographic map of the Aosta Valley[1]

In a geologically context the manganese deposit at St. Marcel (Prabornaz) lies within the Penninic Ophiolite sequence of the Zermatt-Saas unit of the Piemonte nappe *[Griffin, Mottana 1982]*

The Penninic nappe system is part of the alpine collisional belt. The Alps were generated by the Cretaceous to present convergence of the Adriatic continental upper plate. This process also included the subduction of the Mesozoic ocean and the European passive continental margin. The Austroalpine-Penninic wedge represents the collisional zone.

---

[1] Source: *http://www.g26.ch/italien_karte_aostatal.jpg, 10th Oct. 2010*

The forming process of the Alps started by the closure of the Penninic Ocean, which was a side tract of the Central Atlantic Oceanic System. The Penninic Ocean was initiated in the late Triassic by rifting and disjunction of the Austroalpine micro continent from the southern European Plate margin. The sea floor spreading lasted from the middle Jurassic to the early Cretaceous, when the closure started. The oceanic crust got subducted beyond the Austroalpine plates from the late Cretaceous to the Eocene. During its lifetime it was the bond of the Tethys and Atlantic Ocean System.

In general the Alps can be subdivided into two belts, by following the direction of tectonic transport *[Dal Piaz et al. 2003]*: the Europe-vergent belt, a collision wedge of Cretaceous to Neogene age, and the Southern Alps (Adria-vergent), which is a displaced thrust-and-fold belt to the south of Neogene age (see figure 1-2). Both belts are separated by a major fault system called the Periadriatic lineament.

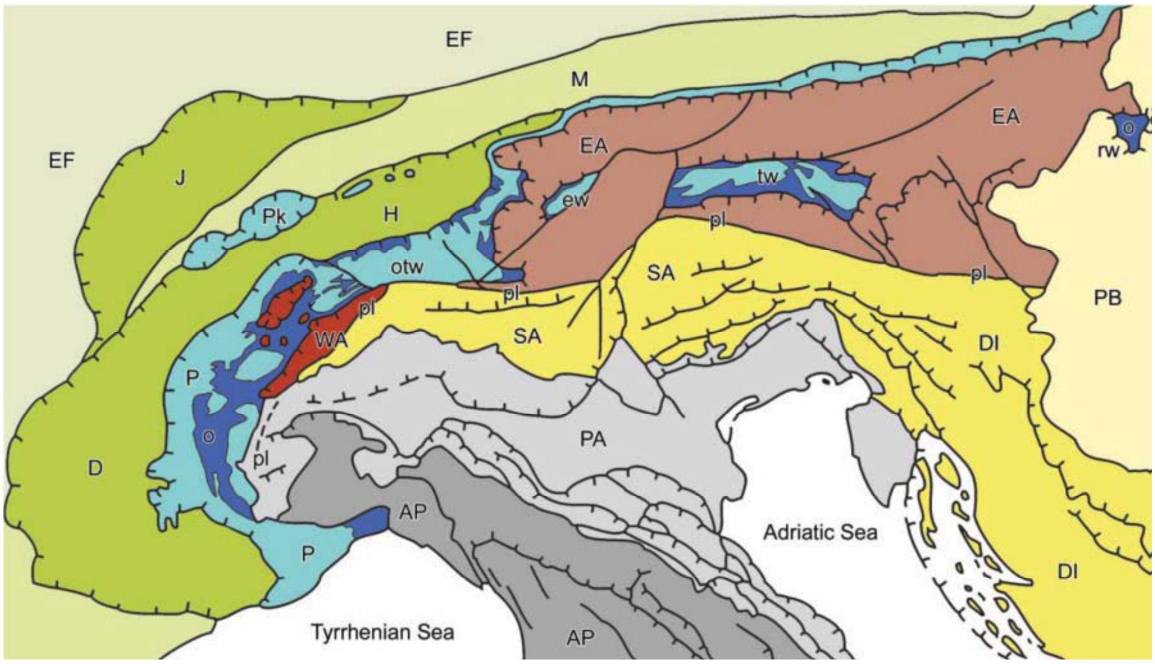

Figure 1-2: **Tectonic map of Alps *[Dal Piaz et al. 2003]*:** (1) Europe-vergent collisional belt: i) Western (WA) and Eastern (EA) Austroalpine; ii) Penninic domain: continental and ophiolitic (o) nappes in western Alpine arc (P) and tectonic windows (otw: Ossola-Ticino, ew: Engadine, tw: Tauern, rw: Rechnitz); Prealpine klippen (Pk); iii) Helvetic-Dauphinois (H-D) domain; iv) Molasse foredeep (M); v) Jura belt (J). (2) Southern Alps (SA), bounded to the north by the Periadriatic lineament (pl). Pannonian basin (PB), European (EF) and Po Valley - Adriatic (PA) forelands, Dinaric (DI) and Apenninic (AP) thrust-and-fold belts.

The Europe-vergent tectonic domains can be split of in three major zones. The Helvetic zone displays the lowermost zone, which derived from the proximal part of the European margin *[Dal Piaz et al. 2003]*. The next tectonic domain is the Penninic zone, a stack of generally metamorphic nappes scraped off the subducting oceanic lithosphere and European passive continental margin *[Dal Piaz et al. 2003]*. At the top is the Austroalpine composite nappe system, which derived from the distal part of the Adriatic passive continental margin *[Dal Piaz et al. 2003]*.

The Austroalpine nappe system can be divided in two general parts, the Western Alps and the Eastern Alps. The Western Alps become subsidence in the area of the Rheine Valley beyond the stack of the eastern alpine nappe system and crops out there in several tectonic windows (i.e. Engading-, Rechnitz- or Tauern-window).

The major units of the western Austroalpine are the Sesia-Lanzo zone and numerous more thrust units grouped as Argand's Dent Blanche nappe *[Dal Piaz et al. 2003]*. These units override and are partly tectonically interleaved with structurally composite ophiolitic Piemont zone *[Dal Piaz et al. 2003]*.

The Piemont zone is part of the Penninic zone, a group of continental and oceanic nappes. Those nappes arrived from the distal European continental margin and the Mesozoic ocean and belonged to the subduction of the lower plate *[Dal Piaz et al. 2003]*. Generally the Penninic zone is built up of a pre-Triassic crystalline basement and a Mesozoic covers. Dal Piaz et al. (2003) classified the Penninic zone from top to bottom:

i. The ophiolitic Piedmont zone
ii. The inner-Penninic Dora-Maria, Gran Paradiso and Monte Rosa continental basement nappes
iii. The middle-Penninic Grand St. Bernand (Briançonnais) composite nappe system
iv. The lower-Penninic nappes of Ossola-Ticino window and outer-Penninic Valais zone, including ophiolitic units and/or flysch nappes, bounded by Penninic frontal thrust
v. The Prealpine klippen, a stack of décollement cover nappes in the French-Swiss Alps

The manganese deposit Prabornaz consists within the ophiolitic Piemont zone, which can be subdivided into two main ophiolithic complexes *[Bearth 1974]*: the Zermatt-Saas zone and the Combinzone.

The Zermatt-Saas zone consist all typically parameters of the oceanic crust and the upper mantle portion *[Bearth 1974]*. It also enclosed a thin layer of sediments with radiolarits. This zone is characterized by an enormous basal complex of completely serpentinized peridotites and a discontinuous band up to 400m thick of eclogitic metagabbros *[Diamond 2001]*. Both are overlain in turn by basaltic metavolcanics with high-P mineral assemblages, which are variable retrogressed to greenschist-facies conditions *[Diamond 2001]*. The overlying rocks are described through a volcano-sedimentary sequence, with locally manganiferous schistose quartzite *[Diamond 2001]*.

The rocks of the Zermatt-Saas zone comprise ultramafics, gabbros and vulcanite. Ultramafics were constant serpintinized *[Bearth 1974]*. Chlorit (in general Brucite) and several generations of antigorite generate the basic compositions of those rocks *[Bearth 1974]*. The most rocks are high in Rutile or Titanite, apatite and ore. Bearth (1974) mentioned that the Zermatt-Saas zone may represent the transition zone of Peridotites to Gabbro.

The basic part of the Combinzone is characterized by serial sediments, which were sedimented at continental crust (Mt. Rosa, Gran Paradiso and Dora Maira) *[Bearth 1974]*. That complex was ride over in the south of Grand Paradiso from the Zermatt-Saas zone. According to the inversion the Combinzone overlies the Zermatt-Saas zone in the north of Grand Paradiso *[Bearth 1974]*.

1.1. Geological setting of the manganese deposit Prabornaz (St. Marcel)

The St. Marcel Valley is a cross-section through the upper portion of the Zermatt-Saas zone *[Diamond 2001]*. Furthermore the St. Marcel Valley contains two overlaying klippen of Austroalpine origin. In the west there is settled the Mt. Emilius klippen and in the east the Glacier-Rafray klippen *[Diamond 2001]*. The deposit itself occurs within the meta-ophiolites of the Piemont nappe, which extends along the entire arc of the Western Alps *[Tumiati et al. 2010]*. To specify it is an external member of the Piemonte Ophiolite nappe *[Diamond 2001]*. It consists to be pre-orogenic and can be characterized as a seafloor-type Mn- and Fe-ore deposit, which was metamorphism during the late Cretaceous and Early Tertiary subduction *[Diamond 2001]*.

The sequence of St. Marcel consists of an oceanic-type ophiolitic basement and a metasedimentary cover belonging to the Piemonte zone *[Tarotti et al. 1986]*. The basement is characterized by Mn-Fe rich metacherts at the bottom, marbles and calcschists at the top (see figure 1-7). These sequences are equivalent to the Upper

Jurassic – Lower Cretaceous supraophiolitic sediments of the Ligurian Apennines *[Martin, Tarotti 1989]*. Diamond (2001) characterized the deposit as syngenetic, which got formed as a result of submarine, volcanic exhalitions.

The manganese concentrations of Prabornaz are restricted to 4x8m thick quartzite unit and (figure 1-3) represent the basal part of the sedimentary cover of the ophiolite suit. Prabornaz is enriched in Mn (up to 38.74 wt% Mn_2O_3) and many trace elements *[Tumiati et al. 2010]*.

Figure 1-3: Braunite ore body, penetrated by small quartzitic fissures and bedded in piemontite (pictured by R. Bakker, July 2010)

The quartzite unit is composed of a sequence of siliceous levels characterized by Mn-bearing minerals reflecting differences in chemical composition and oxygen fugacity inherited from the original sediments. Prabornaz is the most important manganese deposit in the Piemonte nappe. The deposit (figures 1-4, 1-5 and 1-6) is known since 1415 *[Tumiati et al. 2010]* and the mine reaches economic levels of the manganese concentrations *[Diamond 2001]*. There is a diversity of different metamorphic manganese minerals. The ore is restricted to boudinaged quartz-rich layer, which extends over about 100m and ranges from 0.4 to 8m thickness *[Tumiati et al. 2010]*. It is overlain by serpentinite, chlorit-schist and quartz-rich schist. Tumiati et al. (2010) classified the stratigraphy of the deposit in seven levels (see figure 1-7).

Figure 1-4: View to the Prabornaz mine (pictured by R. Bakker, July 2010)

Tumiati et al. (2010) arranged the ore layered body in seven levels. Level 0 represents the footwall, which is in contact with the underlying garnet-bearing glaucophane. The next stratigraphically higher level (Level 1) is named as basal Mn-rich level. It is a braunite- and clinopyroxene-rich layer. The pyroxene there is violan, a violet, Mn-rich variety of diopside. Most of this level has now disappeared, as it was intensively mined for Braunite. Level 2 is the ore-body level. It is dominated by piemontite (a manganese rich epidote mineral), braunite and quartz. This level also contains yellow layers of spessartine-rich garnet. The next level is an irregular emerald-green layer composed of quartz and Cr-bearing, aeginerine-rich omphacite. Tumiati et al (2010) also mentioned that layer as the poorest manganese concentration in the ore-body. Even the quartz-rich layers of the hanging wall containing higher concentrations in manganese than level 3. The following next two levels can be assumed as calderite-rich garnet bearing levels. The garnets are bedded in a quartz-rich matrix with minor hematite. The level 6 is composed of pinkish-orange boudins of quartz, pyroxmangite, strongly zoned garnet and dark-colored manganocummingtonite. The hanging wall of the ore-body (level 7) is buildup of quartz, spessartine-rich garnet, Mn-Ca carbonates, secondary Mn oxids and chlorite. The contact country-rock of the hanging wall is blueschist-facies quartz-rich schist. The total thickness of the ore-body is averaged as four meters.

Figure 1-5: Old entrance of the deposit Prabornaz (pictured by R. Bakker, July 2010)

Figure 1-6: Probably old community rooms of the Prabornaz mine (pictured by R. Bakker, July 2010)

It is very difficult to assess the metamorphic conditions of the manganese deposit, because conventional geothermobarometry and thermodynamic modeling cannot be straightforwardly applied in Mn-rich petrological systems. Tumiati et al. (2010) mentioned an estimated pressure of 2.1±0.3 GPa and a temperature of 550±60 °C. This would place the metamorphic peak for the deposit into the blueschist-facies. Also the presence of glaucophanite with pseudomorphs after lawsonite indicates a p-T evolution across the lawsonite-blueschist subfacies during prograde metamorphism *[Tumiati et al. 2010]*.

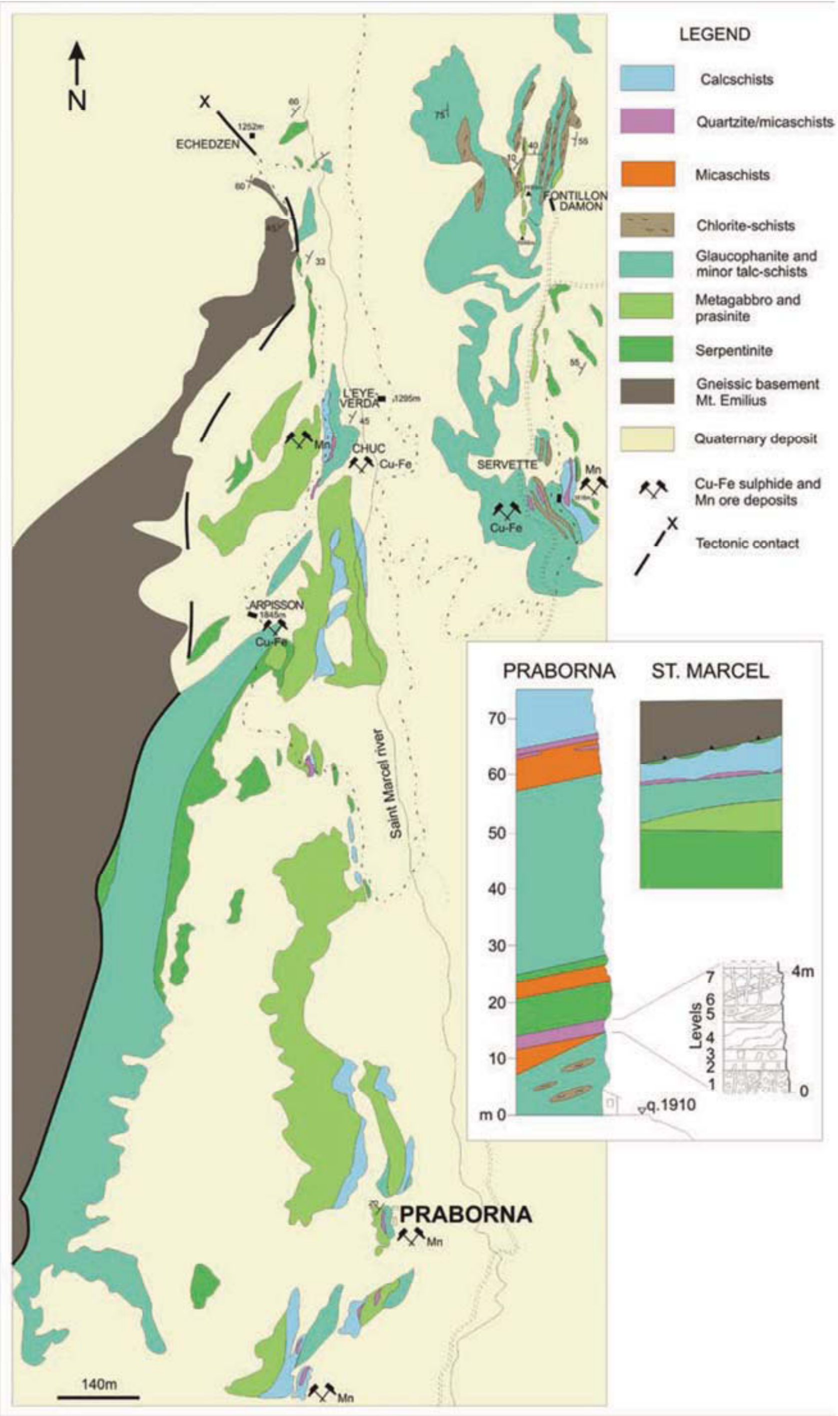

Figure 1-7: Geological map of the St. Marcel valley. The schematic lithostraphigraphy of the whole St. Marcel valley and the detailed sequence of Prabornaz[2].

---

[2] Source: TUMIATI, S.; MARTIN, S.; GODARD, G. (2010): Hydrothermal origin of manganese in the high-pressure ophiolite metasediments of Praborna ore deposit (Aosta Valley, Western Alps); European Journal of Mineralogy; 22; p. 580

1.2. Metamorphism history

The metamorphism history of the ophiolite nappe is complex. It underwent the Eo-Alpine eclogitic metamorphism *[Diamond 2001]*. The alpine metamorphism is characterized by an increasing of temperature and pressure from the west (external) to the east (internal) *[Bearth 1974]*.The tectonical history is in close contact with the metamorphism history.

In general the metamorphism of the ophiolite nappe can be subdivided into three main events and a post metamorphic emplacement of andesitic dykes *[Passchier et al. 1981]*. The four principal equilibrium assemblages seemed to be *[Tumiati et al. 2010]:*

- a primary, higher-p peak assemblage, general characterized by amphibolite facies
- an intermediate blueschist-facies retrograde assemblage
- a late low-p greenschist facies assemblage
- Weathering products.

Passchier et al. (1981) distinguished five generations of folds. F_0 was probably produced of pre-Alpine age and the fold generations F_1-F_4 can be settled of Alpine age *[Passchier et al. 1981]*.

The first metamorphism event is characterized by an amphibolite facies metamorphic assemblage. The preserved amphibolite relicts occur as large lenses *[Passchier et al. 1981]*. Those lenses survived the following metamorphism because they have been too poor in sodium to be converted to eclogites; just their contacts with pegmatite veins and surrounding schists got eclogised *[Passchier et al. 1981]*. The first generation of folding (F_0 folds) can just be observed in the amphibolite lenses. So they folding took place under amphibolites facies condition. Passchier et al. (1981) implicated that those generation of folding probably produced of pre-Alpine age.

The HP-metamorphism was a polyphase event. It can be subdivided into three main stages a pre-kinematic (early) LT blueschist stage, followed by a syn-kinematic HT blueschist to eclogite facies and a closing post-kinematic late eclogite facies *[Martin, Tarotti 1989]*. The first stage is characterized by lawsonite and glaucophane *[Martin, Tarotti 1989]*. Passchier et al. (1981) described two main mineral assemblages a glaucophane-omphacite and jadeite and a glaucophane-almandine composition *[Passchier et al. 1981]*. Frey et al (1974) even mentioned that rutile could be observed. The second stage is deduced from the disappearance of lawsonite *[Martin, Tarotti 1989]*.

The main mineral assemblages of the syn-kinematic phase seemed to be almandine-rich garnets, Mg-Fe chloritoid and the association of glaucophane ± zoiste ± paragonite ± chlorite *[Martin, Tarotti 1989; Frey et al 1974]*. The last phase can be recognized by small recristallized rims of garnet and the development of a new generation of chloritoid *[Martin, Tarotti 1989]*. It is believed, that the first stage a 17 kbar pressure have been reached, but the pressure maximum is attained in the second stage.

The HPLT metamorphism event is aged as Cretaceous *[Frey 1974]*. The K-Ar ages of glaucophane and croissite in Mesozoic ophiolites of the Piemont zone yielded ages of 80-100 Ma *[Frey 1974]*. The mineral assemblages are typical of the earliest Alpine metamorphism event. In pelitic, marly and carbonates rocks, the main minerals are sodic amphibole, garnet, phengit and/or paragonite, chloritoid, lawsonite, jadeite, omphacite, rutile and sphene *[Frey 1974]*. The ultrabasic rocks mainly build up by glaucophane or croissite, lawsonite, pumpellyite, jadeite, aegirine, kyanite and chloritoid *[Frey 1974]*.

During the HPLT metamorphism two generations of folding can be identified *[Passchier et al. 1981]*. F_1 folds represent the first stage and F_2 folds represent the second stage of deformation at the metamorphism event. The first stage of deformation rotated the foliation out of its general orientation *[Passchier et al. 1981]*. These folds become specified as asymmetric folds with sinistral vergence with the exception of some dextral folds on the short limb of larger sinistral folds and locally deformed the mineral assemblages *[Passchier et al. 1981]*. F_2 folds developed during the late stages of the HPLT metamorphism, those folds are disharmonic and vary considerably in orientation *[Passchier et al. 1981]*.

The temperature and pressure conditions for eclogitic assemblages estimated to 500±20℃ at a minimal pressure of 12±1 kbar *[Martin, Tarotti 1989]*. Oherhaensli suggested higher values for the kyanite-bearing eclogitic metabasalts of Zermatt, T=600℃ for p=14 kbar *[see at Oherhaensli 1980 in Martin, Tarotti 1989]*.

The third metamorphism event is represented by greenschist facies assemblages. The approximated pressure is ranged at 3-5 kbar with a temperature at 400-500℃ *[Diamond 2001]*. It is manly developed in the Penninic domain, the grade of the metamorphism decreases from the internal to the external portions of the belt *[Frey et al. 1974]*. The generated minerals are chlorite, green biotite, blue-green amphibole, actinolite, stilpomelane, glaucophane, paragonite and chloritoid *[Frey et al. 1974]*. The crystallization of some of those minerals continued after the main phase of deformation *[Frey et al. 1974]*. Albite seemed to be a very common mineral of this facies, especially in the paraschists and metabasits *[Frey et al. 1974]*. In the highest-grade part of the greenschist facies the albites having an oligoclase rim *[Frey et al. 1974]*. Those rims suggesting that a slightly higher temperature must be reached *[Passchier et al. 1981]*. Low pressure assemblages of this facies can be observed in late veins [Tumiati et al. 2010]. This accumulation is characterized by albite, quartz, K-feldspar, titanite, tremolite, barite, rhodonite, calcite, strontianite, witherite and chlorite. Contemporaneous to the early stages of the greenschist metamorphism event was the fourth main deformation event (F_3 folds) *[Passchier et al. 1981]*. The hinge lines showing a numerous variation of deformation and the folds of this generation are usually recumbent *[Passchier et al. 1981]*.

The F_4 folds are distinguished as the latest generation of deformation. The greenschist facies event is followed by the emplacement of andesitic dykes which are dated at 30-35 Ma *[Passchier et al. 1981]*. It is believed that the last generation of deformation has been contemporaneous with or later than the intrusions *[Passchier et al. 1981]*.

The peak conditions for the metamorphism seem to be T=450-500℃ and p=11-13 kbar *[Diamond 2001]*. Griffin and Mottana (1982) arranged the probably maximum for the pressure and temperature conditions at T=500℃ and p=14 kbar. Martin and Tarotti (1989) defined the late- and post-eclogitic trend for the phengite – phlogopite – albite – microcline – haematite – bearing veins of Prabornaz, at a minimum pressure of 12 kbar for temperature near at 400℃.

Two different kind of deformed rocks from the dump at Prabornaz are illustrated in figure 1-8 and 1-9. Figure 1-8 shows a quartzitic lens with probably spessartine accumulations in an almandine-rich garnet. As it can be seen in figure 1-9 a quartzitic fissure in a piemontite can be seen. The transition from the fissure to the host rock is gradually.

Figure 1-8: Almandine-rich garnet with a quartz and spessartine accumulated lens (pictured by R. Bakker, July 2010)

Figure 1-9: Gradually transition of a quartzitic fissure to the piemontitic host rock (pictured by R. Bakker, July 2010)

2. General aspects about manganese

2.1. Arrangement of the manganese

Manganese is the 12th most abundant elements of earth's crust, about 1000 ppm *[Emsley 2001]*. The enrichment of soils ranges from 7 ppm to 9000 ppm, with an average of 440 ppm *[Emsley 2001]*. Sea water just contains about 10 ppb and the concentration of the atmosphere amount to 0.01 $\mu g/m^3$, but that concentration can be 20 times higher in cities *[Emsley 2001]*. After iron, aluminium and copper, it is the 4th most widely consumed metal *[Weiss 1977]*.

Chemical and physical properties:	
Symbol	*Mn*
Atomic number	*25*
Atomic weight	*54,938 gmol^{-1}*
Oxidation states	***7**, 6, 5, **4**, 5, **2**, 1, -1, -2, -3*
Electronegativity	*1.55 (Pauling scale)*
Atomic radius	*127 pm*
Density	*7,21 gcm^{-3}*
Melting point	*1519 K*
Boiling point	*2335 K*
Mohs hardness	*6*

Table 2-1: Chemical and physical properties of manganese

It is a silver-grey transition metal, resemble to iron (see table 2-1). In his solid form manganese is hard and very brittle. It is very difficult to fuse, but easy to oxidize and its physical property is paramagnetic. There are several stages of oxidation, which occur in manganese. All stages from seven to minus three are possible, but the most common oxidation stages of manganese are Mn^{2+} and Mn^{4+}. Manganese is essential for every living species *[Emsley 2001]*. Various enzymes need manganese for their working, it's also demonstrated to be involved in glucose metabolism, the operation of vitamin B_1 and associated with RNA. Until now the systemic position of manganese in the human body and its function is not well known, but it's essential. The total amount in body is about 12 mg *[Emsley 2001]*. The enrichment of human blood seemed to be at 2-8 ppb, bones vary between 0.2-100 ppm and tissue ranges from 0.2 to 2 ppm *[Emsley 2001]*.

2.2. Manganese Minerals and its behavior

The behavior of manganese is controlled by the oxidation state of the environment. A various number of oxidation states are known of manganese. The range reaches from -3 to 7, but only Mn^{2+} and Mn^{4+} are common in nature. Often both oxidation states occur together in the same mineral or in closely intergrown mineral aggregates *[Maynard 1983]*. There exist a widespread variety of minerals which contain manganese. The economic most important manganese ore minerals are listed in the table below:

Mineral name	Formula	Theoretical Mn-content [%]
Manganite	MnOOH	62
Rhodochroisite	$MnCO_3$	49
Hausmannite	Mn_3O_4	72
Pyrolusite	β-MnO_2	63
Braunite	$Mn^{2+}Mn^{3+}_6(SiO_4)O_8$	64

Table 2-2: Most important manganese ore minerals

2.3. Manganese and its uses

Manganese has a widespread range of use. Due to the certainty that manganese is essential for human beings and general for all living species, it is added to fertilizers and animal feedstuff. Even Pliny the Elder († 79 AD) reported from a black powder that glass-makers used to make their product crystal clear *[Emsley 2001]*. During the Pharaonic days it was appropriate as a pigment *[Weiss 1977]*. Due to its several oxidizing stages manganese oxides adopt a multitude of color, that's why it also used for colorizing glass.

Manganese metal is too brittle, but as an addition to steel, it improves the strength of the steel, working properties and wear resistance *[Emsley 2001]*. 95% of the whole mined manganese ore goes into alloys, preliminary steel (see table 2-3). Manganese steel itself contains about 13% manganese; it is a very keen kind of steel. The end use of those steel is for railway tracks, earthmoving machinery, safes, helmets, rifle barrels, bars of prison cells, etc. *[Emsley 2001]*.

Primary **manganese (II) oxide** is a component in the electrolyte paste of zinc-carbon batteries, to prevent the corrosion of the carbon electron. The addition of manganese in that case avoids building up of hydrogen gas next to the electrode. Nowadays manganese (II) oxide can be more likely found in rubbers or as a catalyst in industry. It is one of the two commercial most produced manganese products *[Emsley 2001]*. The other is **manganese (II) sulphate** *[Emsley 2001]*. It is essential for the electrochemical manufacture of manganese metal. Another use of manganese (II) sulphate would be the production of the fungicide Maneb (a manganesedithiocarbonate derivate) *[Emsley 2001]*. In general **manganese (II) oxides** applies for fertilizers and ceramics. The starting material for producing other manganese products or compounds is **manganese carbonate**. **Potassium permanganate** get constitute for removing organic impurities from waste gases and effluent water.

Rank 2008	***Rank 2007***		***Country***	***Production 2008 metr.t.***
1	2	↑	Rep. of South Africa	2.991.002
2	3	↑	Australia	2.304.400
3	1	↓	China	2.200.000
4	4		Gabon	1.625.000
5	8	↑	Brazil	1.284.000
6	5	↓	Kazakhstan	1.192.800
7	6	↓	India	994.080
8	7	↓	Ukraine	910.000
9	9		Ghana	381.543
10	14	↑	Malaysia	257.604
11	10	↓	Mexico	171.773
12	11	↓	Georgia	99.000
13	13		Cote d'Ivoire	74.060
14	24	↑	Thailand	53.280
15	16	↑	Morocco	51.143
16	12	↓	Iran	41.293
17	17		Russia (Europe)	17.600
18	15	↓	Namibia	14.119
19	18	↓	Hungary	13.386
20	19	↓	Turkey	12.000
21	20	↓	Romania	8.904
22	21	↓	Bulgaria	8.195

Rank 2008	***Rank 2007***		***Country***	***Production 2008 metr.t.***
23	25	↑	Russia (Asia)	4.400
24	23	↓	Egypt	2.928
25	22	↓	Chile	1.529
26	26		Bosnia Herzigovina	500

Table 2-3: Manganese production 2008 *[World Mining Data 2009]*

3. Mineralogy of St. Marcel

3.1. Principals of the used measurement methods

3.1.1. Preparation of samples and Microscopy

For the description and characterization of the mineralogy and petrology, thin and thick sections were taken from selected samples. Those samples were analyzed via reflected-light and transmitted light microscopy. An Olympus BX40 microscope was used, and occasionally a Zeiss. The appropriated Olympus objectives were: MSPlan 2.5 0.07, MPlan 4X; MPlan 5X / 0.10; MPlan 10X / 0.25; MPlan 20X / 0.40; MPlan 50X / 0.75; MPlan 100X / 0.90. The microscope was equipped with an uEye camera system.

3.1.2. RAMAN

The Raman spectroscopy uses the physical effect of scattered light. If monochromatic light irradiates molecules or crystal lattices, the light becomes scattered. According to the primary light source, in this case a green laser beam with a wavelength of λ=532.02nm, the monochromatic light gains or loose energy according to the bonding in the abated sample.

The main effect is the Rayleigh scattering: photons which aren’t absorbed by the sample and scattered back in an elastic way without any changes in their wavelength. Another effect can be observed, the Raman effect. It is inelastic back scattering of the photons, when they impacting at swinging molecules. By this impact the photon emits a part of its energy to the molecule and its frequency decrease. The decrease is for every kind of molecule specific and characteristic. The back scattered photon becomes now a new wavelength, which is a little bit longer than the wavelength of the primary beam. The difference of the primary photon beam to the emitted wavelength is called the Stokes diffusion or the Raman effect. The intensity of the Raman effect decreases 10^3 to 10^4 times in comparison to the Rayleigh scattering (see figure 3-1).

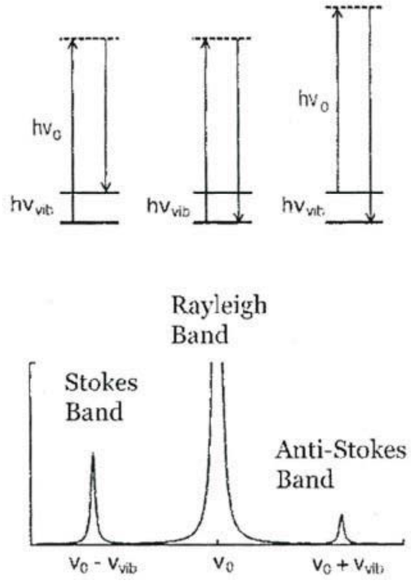

Figure 3-1: Rayleigh and Raman effects [3]

Figure 3-1 describes two different Raman effects. The Stokes band is the wavelength, if the photon emits a part of its energy to the molecule. The Anti-Stokes diffusion can be observed when the photon impact at a vibrating molecule and increases scattering its energy. The Anti-Stokes is mirroring the Stokes at the Rayleigh band. For normal use the Stokes scattering is detected, because the intensity of the Stokes band is higher than the intensity of the Anti-Stokes band, due to probability principles.

For the measurements in this thesis a Jobin Yvon LabRAM with a combined Olympus BX40 microscope was used. The apparatus was connected with a computer. The analysis occurred with the LabSpec software. The used Nd-YAG laser (green) had a wavelength of 532.02 nm and a power of 2 mW. The maximum of possible measurement is at 64.000 cnt. Calibration of Raman is carried out by a silicon standard and polyethylene.

---

[3] Source: http://131.104.156.23/Lectures/CHEM_207/vibrational_spectroscopy, 12th April 2011

3.1.3. SEM (Scanning Electron Microscopy)

The basic principal of a Scanning Electron Microscope is an electron beam, which is scanning the surface in a raster. If the electron beams impacting the sample surface, interactions are generated. Those interactions can be detected. The primary use for SEM is topographical reason, because a maximum of enlargement of 1.000.000:1 can be reached. Derived signals can also be used for getting information's about the chemical composition, crystalline structure and the orientation of the analyzed material. Another advantage of using SEM is that the sample doesn't get destroyed during the measurement.

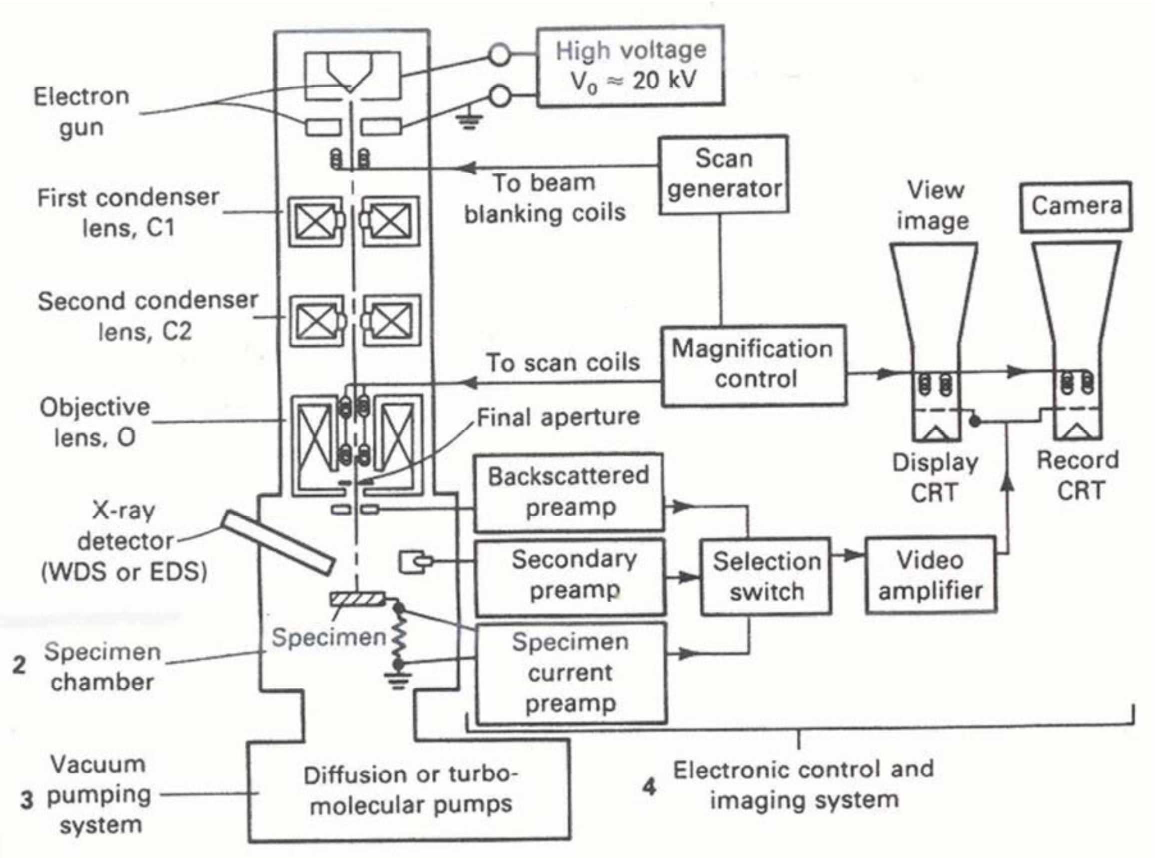

Figure 3-2: Schematic cross-section of a scanning electron microscope[4]

The Microscope is built up by three main groups of components (see figure 3-2):

---

[4] Source: http://www.nhml.com/i/resources_NHML_Scanning-Electron-Microscopes_fig1_lg.gif, 18th April 2011

- Electron-optical column
- Vacuum system
- Signal detection and display group

The electron column consists of an electron gun and two to four lenses, depending on the design. There are two different systems for producing the electron beam. By the one system the conductor is hair-pin shaped and made out of wolfram or a LaB_6-crystal. The conductor is heated and starts to emit electrons. At a stress field of 8 to 30 kV, the electrons become accelerated. The other system for producing the electron beam uses the technique of field emission. The field emission gun is made out of very fine cone ending wolfram crystal. By the application of a field force, the electrons get emitted. There are two ways of field emission: the cold and the thermal field emission. At the cold field emission the cathode doesn't get heated, in contrast to the thermal field emission, where the cathode is minimal heated. The heated principal leads to a higher intensity of radiation and produces a high quality of the pictures at a less acceleration. The primary electron beam is focused by the condenser lenses. Usually the last lens deflect the beam in x and y axis so that it scans raster over a rectangular area of the sample surface.

The vacuum system conduced to avoid a deflection or collision of the electrons with air or dust particles. In contrast the environmental scanning electron microscope (ESEM) uses the effect of air and dust particles. Therefore this effect is disposed of amplifying the signals and to simulate real condition for the measurement.

For SEM analysis the sample has to be coated with a conductive material, in this case carbon coating has to be used. The coating produces a maximum of conductivity at the sample surface. If the primary electrons beam impacts at the sample a multitude of signals are produced: secondary electrons (SE), Backscattered electrons (BSE), characteristic X-rays and catholuminiscence. Depending on the measurement model all kind of reflected electrons can be detected or a few of them. For this thesis just back-scattered electrons have been measured. Back-scattered electrons are the results from elastic scattering interactions with specimen atoms. Elements with a higher atomic number backscattering electrons more strongly than light elements, that's why higher elements are brighter in a backscattering electron image.

The Magnification in a SEM can't be controlled by the lenses. The function of the lenses is to focus the electron beam, so the magnification results from the ratio of the raster dimensions, higher magnification followed from reducing the size of the raster on the specimen.

The SEM measurements were done at the University of Oulu *(Finland)* with the JSM 6400 Scanning Microscope from JEOL. The used analyzing system was an Oxford IDS-System.

3.1.4. Electron microscopy and X-ray Fluorescence Spectroscopy

The electron microscopy is operating like the scanning electron microscope. More precisely the scanning electron microscope is a variety of the electron microscope. They contend the same three main components, an electron-optical column, a vacuum system and a signal detection and display group (see figure 3-1).

The sample is placed in the vacuum chamber. A focused monochromatic electron beam fire at the sample surface. The energy of this electron beam ranges from 5-50 keV. A part of this electron beam penetrates the sample and releases X-rays. Those X-rays can be detected in two different ways. One opportunity is the identification with the aid of the element specific wavelength (wavelength dispersive system) or with the aid of their specific energy (energy dispersive system). With both methods element identification is possible.

The WDS (wave dispersive system) is used for quantitative analysis. Basic principle is Bragg's law:

$$n * \lambda = 2 * d * \sin\theta$$

Where	n	*is order of diffraction,*
	λ	*is wavelength,*
	d	*is distance of lattice planes and*
	$\sin\Theta$	*is angle of refraction between the x-ray and the lattice plane.*

Summarized the Bragg's law describes the cohesion of X-ray and crystal lattice. In general X-rays soak crystal lattice, but a short amount diffracts at the lattice. That angle of refraction is for every mineral characteristic. WDS spectrometers use these effects. Moveable crystals with known d-data, also called monochromes, offer the possibility for accurate measurements at a defined wavelength. The emitted wave package is proportional to the element frequency in the sample.

The EDS (energy dispersive system) is used for qualitative analysis. Therefor the detectors register the X-ray as a function of their energy, a big advantage for fast identification. But the analytical exactness is much lesser than those of the WDS.

3.1.5. Microthermometry

The microthermometry is a method for studying fluid inclusion more intensive, because phase transitions can be observed. One of the phase transitions is the melting point and the other is the homogenization point. The melting point is defined as that temperature when solid phase changes in liquid phase. The homogenization point is defined when the liquid phase transit in a gas phase or a super critical fluid. Therefor the combined heating and cooling table become conductive heated. Just temperatures which can be observed for the melting point or the homogenization point during a heating cycle are significant, due to the metastabilities during a cooling cycle.

For the measurements a LINKHAM MDS 600 heating and cooling table in combination with an Olympus BX60 microscope was used. The LINKHAM stage is connected with a computer; with its aid and the software program LINKSYS32 the melting and homogenization temperatures can be observed. The cooling of the stage occurred with liquid nitrogen. The calibration happened with synthetic CO_2 fluid inclusions (T_mCO_2 = -56.6℃) and distilled water inclusions (T_mH_2O = 0.0℃, T_hH_2O = 374.0℃).

The preparation of the sample applied by both side polished thick sections, how got solved with acetone from their specimen holder. Relevant areas of fluid inclusions have been selected and analyzed with Raman. Raman measurements allowed qualitative validity about the gas and fluid phases which are cached in the inclusions. Next step was the measuring of the homogenization and melting temperature with the LINKHAM stage.

3.2. Results and description of the Mineralogy and Petrology

For the description of the mineralogy and petrology of the manganese ore body at St. Marcel, ten characteristic samples have been selected. Eight out of ten samples are from the dumping at Prabornaz mine (GPS coordinates: N 45°40’46.6’’ E 007°27’00.1’’ altitude 1795m) (figure 3-3). Only sample SM42 and SM48 are taken from the Servette mine (GPS coordinates: N 45°42’06.9’’ E 007°27’19.6’’ altitude 1735m) (figure 3-4). Sampling was carried out under supervision of a.o. Prof. R.J. Bakker.

Figure 3-3: Dump of Prabornaz (pictured by R. Bakker, July 2010)

Figure 3-4: Servette mine (pictured by R. Bakker, July 2010)

3.2.1. SM20

Already the tool holder is characterized through dark red micas in a blackish matrix. Those micas are sparkling dark red to violet and having a size up to three millimeters. It seemed as they are “swimming” in the black matrix. The black minerals are fine grained and they are also a little bit sparkling. At the first interpretation of the hand piece, for the main blackish matrix the assumption clinopyroxene has been made. The sample is divided by a one to two millimeter thick fissure, which is filled up with quartz. In general red micas are more or less parallel orientated, to the foliation, which is locally folded resulting in a variable orientation of red micas.

Figure 3-5: Scanned thin section SM20 (length of the picture correlates to 2.8cm x 4.8cm)

The scanning electron microprobe analysis specified the blackish matrix as two different types of clinopyroxenes. One of the clinopyroxenes can be named as augite – $(Ca,Na)(Mg,Fe^{2+},Al,Fe^{3+};Ti)[(Si,Al)_2O_6]$. In the microscope the augite minerals look like brownish near to golden blocks. They show pleochroism and colors of interference.

Primary they are found next to quartz rich areas. The other clinopyroxene is aegirine-augite (richer in Na und Fe^{3+}).

The reddish mica in this sample is alurgite – $K_2(Mg,Al)_{4\text{-}5}(Al,Si)_8O_{20}(OH)_4$, a variety of muscovite. They show a leave-shaped habitus and it can identify by color and pleochroism (bright orange perpendicular to cleavage, bright pink parallel to cleavage). The alurgite crystals show interference colors of the second order. They are reaching up to two millimeters ample blocks and occur together with the augites. It seemed that they are alteration products of augites. Different reasons for this deduction are that no brownish augitic material can be found in the pinkish area; just a few single augite minerals can be detected in the alurgite dominated areas. The pinkish mineral phase show the same habitus like the augites. Another reason for this theory is the monitoring of a brownish "fog", which is surrounding alurgite. They are having a large amount of opaque inclusions. That opaque mineral phases are hollandite – $Ba(Mn_{4+},Mn_{2+})_8O_{16}$, braunite – $Mn^{2+}Mn_6^{3+}(SiO_4)O_8$ and cryptomelane – $K(Mn^{4+},Mn^{2+})_8O_{16}$. They are very fine grained and strongly intergrown.

Other minerals which could be identified are calderite – $(Mn^{2+},Ca)_3(Fe^{3+},Al)_2(SiO_4)_3$, greenovite – a manganese bearing variety of titanite – $CaTi(SiO_4)O$, hematite – Fe_2O_3, orthoclase – $KAlSi_3O_8$, albite – $NaAlSi_3O_8$, aluminoceladonite – $K(Mg,Fe^{2+})Al(Si_4O_{10})(OH)_2$ and quartz – SiO_2.

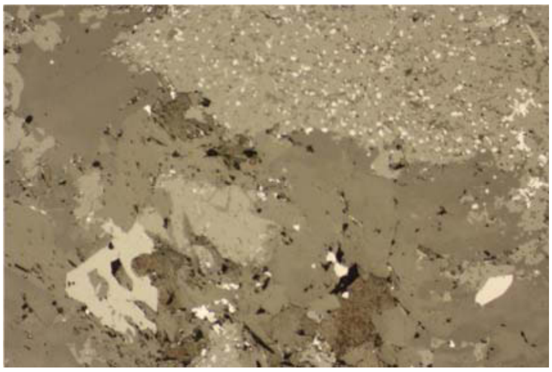

Figure 3-6: Greenovite, braunite, calderite and aegirine-augite in reflected light (10 times extension, length of the picture correlates to 3.6 millimeters)

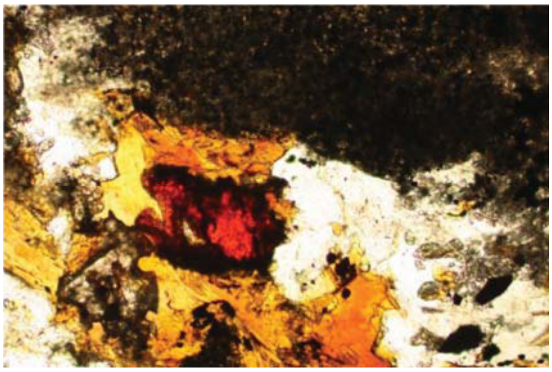

Figure 3-7: Greenovite, braunite, calderite and aegirine-augite in transmitted light (10 times extension, length of the picture correlates to 3.6 millimeters)

The minerals in figure 3-6 and 3-7 were analyzed with the electron microprobe. The dark red mineral is calderite. Next to the calderite, bedded in a brownish to golden phase, is the manganese bearing variety of titanite named greenovite. At the lower right corner there is an opaque mineral, which is at the reflected light figure much brighter than the titanite. Those bright grains in figure 3-6 can be identified as braunite. At the right top in figure 3-7 can be seen a dark brown to grey phase. This mineral is interstratified with small braunite grains and can be specified as aegirine-augite. The golden mineral phase wasn't measured via microprobe, but in comparison with other measuring points of minerals with the same properties, it can be named as augite.

Analysis	1	2	3	4	10	11
Mineralphase	*Braunite*	*Braunite*	*Braunite*	*Greenovite*	*Alurgite*	*Alurgite*
Na_2O	-	0,02	-	0,09	-	0,01
MgO	0,47	0,61	0,49	-	7,40	7,45
Al_2O_3	0,08	0,07	0,06	0,31	15,86	15,32
SiO_2	9,81	10,07	9,29	28,27	53,72	52,80
SO_3	-	0,00	0,03	-	0,03	0,02
K_2O	0,34	0,40	0,38	0,26	9,20	9,32
CaO	1,09	3,50	0,64	34,38	0,00	-
TiO_2	-	0,09	0,02	35,68	0,44	0,37
V_2O_3	0,05	0,00	0,02	0,34	0,11	0,03
Cr_2O_3	-	-	0,00	-	-	0,00
MnO	7,44	3,57	7,31	0,43	1,84	2,14
Mn_2O_3	76,96	76,66	77,97	-	-	-
FeO	0,93	1,63	0,95	0,62	1,32	1,20
Sum	**97,17**	**96,62**	**97,17**	**100,38**	**89,92**	**88,65**
Oxygen	12	12	12	5	20	20
Na^+	-	0,00	-	0,01	-	0,00
Mg^{2+}	0,07	0,09	0,08	-	1,68	1,72
Al^{3+}	0,01	0,01	0,01	0,01	2,85	2,79
Si^{4+}	1,01	1,03	0,96	0,90	8,20	8,17
S^{6+}	-	0,00	0,00	-	0,00	0,00
K^+	0,04	0,05	0,05	0,01	1,79	1,84
Ca^{2+}	0,12	0,38	0,07	1,18	0,00	-
Ti^{4+}	-	0,01	0,00	0,86	0,05	0,04
V^{3+}	0,00	0,00	0,00	0,01	0,01	0,00

Analysis	1	2	3	4	10	11
Mineralphase	*Braunite*	*Braunite*	*Braunite*	*Greenovite*	*Alurgite*	*Alurgite*
Cr^{3+}	-	-	0,00	-	-	0,00
Mn^{2+}	0,65	0,31	0,64	0,01	0,24	0,28
Mn^{3+}	6,02	5,97	6,11	-	-	-
Fe^{2+}	0,08	0,14	0,08	0,02	0,17	0,16

Table 3-1: Selected scanning microscope analyses and microprobe analyses of SM20 (Oxides are given in mass%, ionic composition is calculated according to the number of oxygen atoms in general mineral formulas. Total content of MnO and Mn_2O_3 are calculated according to the method of Droop 1987)

The measured braunites also show a small content of magnesium, potassium, iron, aluminum and calcium (see table 3-1). Measurement three also show a minor amount Cr_2O_3. These results are very similar to those of Tumanti et al. (2010), where braunite is mentioned as one of the major rock forming minerals at Prabornaz.

Aegirine-augite pyroxenes are only observed in SM20, Table 3-2 illustrates the variation in composition. They are relatively enriched in Na and Fe.

Na_2O	8,10 - 10,91	**Na^+**	0,61 - 0,76
MgO	4,03 - 4,74	**Mg^{2+}**	0,22 - 0,27
Al_2O_3	2,01 - 4,02	**Al^{3+}**	0,09 - 0,17
SiO_2	51,42 - 55,58	**Si^{4+}**	1,98 - 2,00
CaO	6,38 - 7,28	**Ca^{2+}**	0,24 -0,30
TiO_2	< 0,16	**Ti^{4+}**	< 0,005
MnO	< 0,42	**Mn^{2+}**	< 0,01
FeO	0,39 - 5,85	**Fe^{2+}**	0,01 - 0,19
Fe_2O_3	18, 58 -23,05	**Fe^{3+}**	0,54 - 0,63

Table 3-2: Variation of composition of aegirine-augite in mass percent. (Oxides are given in mass%, ionic composition is calculated according to six oxygen atoms Total content of FeO and Fe_2O_3 are calculated according to the method of Droop 1987)

3.2.2. SM21

The sample SM21 is rich in quartz and garnet with large amounts of opaque material. The garnet is fine grained and individual grains are not detectable with normal loupe of 10x magnification. The garnet is yellowish colored and probably a spessartine or calderite. Masses of fine-grained garnets and the opaque material are intergrown. At other parts of the sample bands of quartz are alternating the garnet-rich layer. In general, a foliation is not well developed in this section.

Figure 3-8: Scanned thin section SM21 (length of the picture correlates to 2.8cm x 4.8cm)

The Garnet grains are brittle deformed in multiple parts. Most of the generated fine fissures are filled with quartz, but some contain also a second phase of garnet rich material. With the aid of the scanning electron microprobe the yellow garnet grains can be identified as spessartine – $Mn_3^{2+}Al_2(SiO_4)_3$.

The distribution of quartz and spessartine grains can be visualized with an optical microscope or with an electron image of scanning electron microscope (figure 3-9).

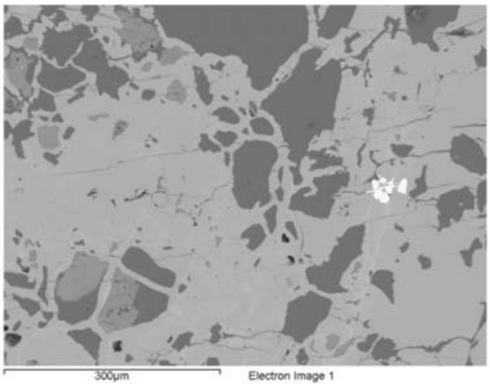

Figure 3-9: Electron image SM21.1, dark grey is quartz, bright grey is spessartine

The dark grey minerals in figure 3-9 are the embedded quartzes which are surrounded by spessartine. The bright accumulation next to the right boarder is an iron oxide (hematite or magnetite).

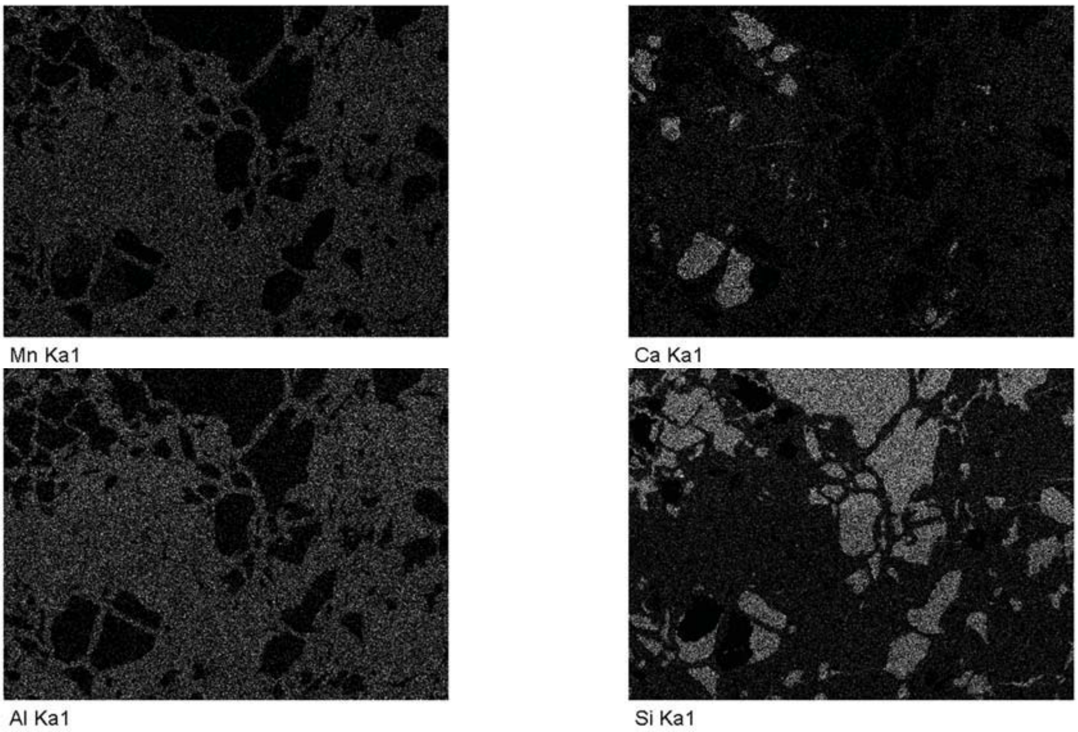

Figure 3-10: Landscape imagining of figure 3-9 by scanning electron microscope analyses (Ka in images complies with Kα).

Figure 3-10 illustrates the Mn, Ca, Al and Si distribution from figure 3.9. The Ca-rich grain is a calcite, probably rich in manganese. The opaque mineral phase is goethite. A brittle ductile transition can be observed (figure 3-12).

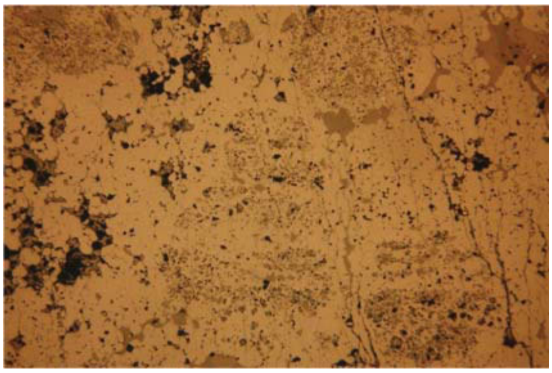

Figure 3-11: Brittle ductile deformation of garnets in reflected light (10 times extension, length of the picture correlates to 3.6 millimeters)

Figure 3-12: Brittle ductile deformation of garnets in transmitted light (10 times extension, length of the picture correlates to 3.6 millimeters)

Analysis	17	18	19	20
Mineralphase	*Spessartine*	*Spessartine*	*Spessartine*	*Calderite*
MgO	0,50	-	-	-
Al_2O_3	19,90	19,44	20,14	13,49
SiO_2	36,99	36,97	37,03	35,72
CaO	5,58	3,50	5,40	3,37
TiO_2	0,45	-	0,38	0,62
MnO	34,64	38,45	38,19	39,08
FeO	1,51	0,78	-	8,89
Fe_2O_3	2,54	1,98	-	-
Sum	**102,10**	**101,12**	**101,15**	**101,17**
Oxygen	**24**	**24**	**24**	**24**
Mg^{2+}	0,12	-	-	-
Al^{3+}	3,76	3,72	3,82	2,64
Si^{4+}	5,92	6,02	5,98	5,96
Ca^{2+}	0,96	0,60	0,93	0,60
Ti^{4+}	0,06	-	0,04	0,08
Mn^{2+}	4,68	5,30	5,72	5,50

Analysis	17	18	19	20
Mineralphase	*Spessartine*	*Spessartine*	*Spessartine*	*Calderite*
Fe^{2+}	0,20	0,12	-	1,24
Fe^{3+}	0,30	0,24	-	-

Table 3-3: Selected scanning microscope analyses and microprobe analyses of garnets from SM21 (Oxides are given in mass%, ionic composition is calculated according to 24 oxygen atoms. Total content of FeO and Fe_2O_3 are calculated according to the method of Droop 1987)

The calderite is relatively enriched in Fe compared to spessartine, whereas the Ca and Al contents are lower. Both types of garnets occur in this section.

Analysis	17	18	19	20
Almandine	9,05	6,17	0,00	17,31
Spessartine	77,37	86,00	87,61	76,12
Pyrope	1,11	0,00	0,00	0,00
Grossular	12,47	7,82	12,39	6,57

Table 3-4: Calculations of end members of measured garnets from table 3-3, in percentages

All garnet analyses show enrichments in spessartine (table 3-4). Even the calderite analysis, analysis number 20, has a very high content in the end member of spessartine (76.12%), but is richer in the almandine end member in comparison to the other spessartine analyses of table 3-4.

3.2.3. SM22

The sample can be described as a quartz – piemontite - braunite rich rock, which contains minor amounts of pyroxene (accessorial). Piemontite - $Ca_2(Al_2Mn^{3+})(Si_2O_7)(SiO_4)O(OH)$ are elongated crystals within pyroxenes. A preferred orientation of crystals was not observed in the sample. With a more detailed view two accessorial minerals can be observed. The first is a radial grain assemblage of violet minerals of violet minerals settled in quartz. Unfortunately this mineral phase couldn't be caught in the thin section, because it is a brittle phase and just localized at the surface of the sample. The extension of this mineral assemblage is more or less circular with a diameter of 0.9 to 1.7 centimeters. By reflection with the loupe the minerals are columnar grown from a point astral growing. This mineral phase is violane – $CaMgSi_2O_6$, a manganese-rich variety of diopside. The second mineral phase has a white to pale violet color, which is probably a slight altered violane.

Figure 3-13: Scanned thin section SM22 (length of the picture correlates to 2.8 x 4.8cm)

The mineral phases are also analysed with an optical microscope. The red marked area in figure 3-13 indicates the location of the white to pale violet mineral phase. With polarized light a pleochroism of the second order (pink to green) is visible. Microprobe analyses allowed a classification of macfallite $Ca_2(Mn^{3+},Al)_3(Si_2O_7)(SiO_2)(OH)_3$, a sorosilicate (Mn-rich pumpellyite).

The general impression of this thin section is a stong intergrow between piemontite, pyroxens and opaque minerals, in general braunite.

Figure 3-14: Diopside surrounded by quartz in transmitted light (10 times extension, length of the picture correlates to 3.6 millimeters) A brittle ductile transition can be observed

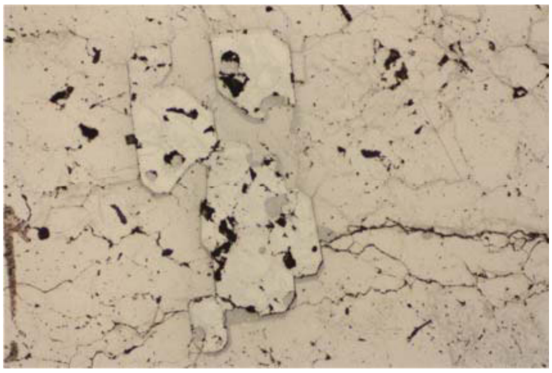

Figure 3-15: Diopside surrounded by quartz in reflected light (10 times extension, length of the picture correlates to 3.6 millimeters) A brittle ductile transition can be observed

The area of figure 3-14 and 3-15 has been analyses via scanning electron microscope. These translucent greyish minerals are diopside (violane) grains bedded in quartz (see figure 3-14). Diopsides appear like small crystals in the quartz rich area, in the top right corner (see figure 3-13). They are generally fine grained; locally those diopside grains are larger (figure 3-14). Diopsides are widespread in the transition from piemontite rich areas to the quartz rich areas.

Piemontites of this sample are unremarkable in this sample. They are fine grained and occur together in matrix of braunites and pyroxenes.

Some selected analyses can be seen in table 3-5. A relative high content of wolfram was measured in the piemontite analyses. The origin of the wolfram is unknown. Even the comparison with piemontite measurements of Tumanti et al. 2010 poses questions, because Tumanti et al. 2010 had no results of wolfram in their analyses. Precise interpretation follows in the chapter “discussion and conclusion”.

Analysis	25	26	27	28	29
Mineralphase	*Macfallite*	*Macfallite*	*Piemontite*	*Diopside*	*Diopside*
Na_2O	-	0,01	-	2,47	1,78
MgO	0,03	0,01	-	15,22	16,53
Al_2O_3	14,06	11,78	18,12	1,25	0,38
SiO_2	34,47	34,00	37,63	57,44	56,33
K_2O	0,14	0,14	1,34	-	-
CaO	24,54	22,96	19,48	21,58	23,25
TiO_2	0,02	-	-	-	-
V_2O_3	0,03	-	-	-	-
Cr_2O_3	0,00	0,00	-	-	-
MnO	-	-	2,58	0,79	0,46
Mn_2O_3	15,49	17,56	13,24	-	-
FeO	2,99	5,14	2,39	1,67	3,65
Fe_2O_3	-	-	-	2,10	-
WO_3	-	-	3,77	-	-
Sum	**91,78**	**91,61**	**98,54**	**102,51**	**102,39**
Oxygen	14	14	12,5	6	6
Na^+	-	0,00	-	0,17	0,12
Mg^{2+}	0,00	0,00	-	0,80	0,87
Al^{3+}	1,44	1,23	1,77	0,05	0,02
Si^{4+}	3,00	3,01	3,11	2,03	1,99
K^+	0,02	0,02	0,14	-	-
Ca^{2+}	2,29	2,18	1,72	0,82	0,88
Ti^{4+}	0,00	-	-	-	-
V^{3+}	0,00	-	-	-	-
Cr^{3+}	0,00	0,00	-	-	-
Mn^{2+}	-	-	0,18	0,02	0,01
Mn^{3+}	1,03	1,18	0,83	-	-
Fe^{2+}	0,22	0,38	0,17	0,05	0,11
Fe^{3+}	-	-	-	0,06	-
W^{6+}	-	-	0,08	-	-

Table 3-5: Selected scanning microscope analyses and microprobe analyses of SM22 (Oxides are given in mass%, ionic composition is calculated according to the number of oxygen atoms in general mineral formulas. Total content of MnO and Mn_2O_3 or FeO and Fe_2O_3 are calculated according to the method of Droop 1987)

3.2.4. SM24

The sample is similar to sample SM22, with the same mineral assemblage. The sample SM24 is made out of piemontite, quartz and braunite (figure 3-14). The mineral grains are reaching sizes up to one to two millimeters. In the hand piece the piemontite crystals are dark red to violet.

Figure 3-16: Scanned thin section SM24 (length of the picture correlates to 2.8 x 4.8cm)

The single piemontite grains are combined to larger piemontite assemblages. It’s difficult to distinguish between the single grains. The same observation can be done for the braunite grains. Those bigger sized grain assemblages are affected by cataclastic cracks and those fissures are filled with quartz. Partially are the braunite grains included in piemontite.

Their color of pleochroism of piemontite in the transmitted light microscope is a strong orange to dark red. Consequently colors of interference can’t be distinguished.

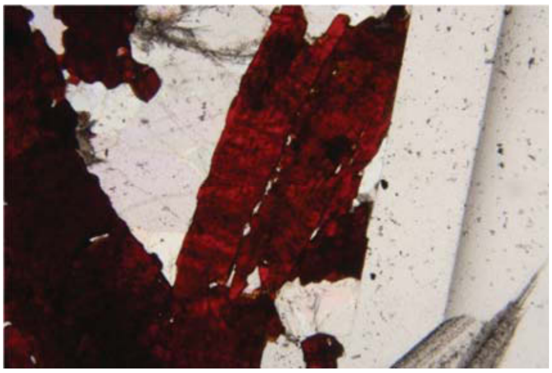

Figure 3-17: Piemontite bedded in quartz in transmitted light (10 times extension, length of the picture correlates to 3.6 millimeters)

Analysis	33	34	35	36	37	38
Mineralphase	*Piemontite*	*Piemontite*	*Piemontite*	*Piemontite*	*Piemontite*	*Piemontite*
Al_2O_3	18,50	18,01	18,61	18,42	17,80	18,54
SiO_2	36,45	35,70	36,17	35,92	35,94	36,22
CaO	21,69	22,28	21,66	21,73	21,63	21,87
MnO	0,64	16,60	0,73	0,69	0,91	15,39
Mn_2O_3	18,49	-	18,30	16,88	17,59	-
FeO	2,23	2,07	2,16	2,91	2,70	2,78
WO_3	1,92	2,30	2,23	3,32	3,13	2,19
Sum	**99,91**	**96,96**	**99,87**	**99,86**	**99,70**	**96,99**
Oxygen	12,5	12,5	12,5	12,5	12,5	12,5
Al^{3+}	1,77	1,75	1,79	1,78	1,72	1,79
Si^{4+}	2,96	2,94	2,95	2,94	2,95	2,97
Ca^{2+}	1,89	1,96	1,89	1,91	1,91	1,92
Mn^{2+}	0,04	1,16	0,05	0,05	0,06	1,07
Mn^{3+}	1,14	-	1,13	1,05	1,10	-
Fe^{2+}	0,15	0,14	0,15	0,20	0,19	0,19
W^{6+}	0,04	0,05	0,05	0,07	0,07	0,05
Σ Mn	1,19	1,16	1,18	1,10	1,16	1,07
Σ Fe	0,15	0,14	0,15	0,20	0,19	0,19
Σ Mn : Σ Fe	7,91	8,12	7,90	5,50	6,13	5,61

Table 3-6: Scanning electron microscope analyses of Piemontite from SM24 (Oxides are given in mass%, ionic composition is calculated according to 12.5 oxygen atoms. Total content of MnO and Mn_2O_3 are calculated according to the method of Droop 1987)

The piemontite analyses of SM24 show similar high contents of wolfram as the analyses in sample SM22. Piemontites with low iron content have also low wolfram content.

At the first look it seemed that piemontites and braunites are crystallized simultaneously, and both are simultaneously deformed. Piemontites occur in braunites and otherwise braunites in piemontite. Both minerals can be found as relicts in the other major assemblage. Both mineral phases are cataclastic disturbed. Most of the braunites offer a small boarder of accretion with clear-cut brighter refraction. Scanning electron microscope analysis showed that those brighter rims are also braunites.

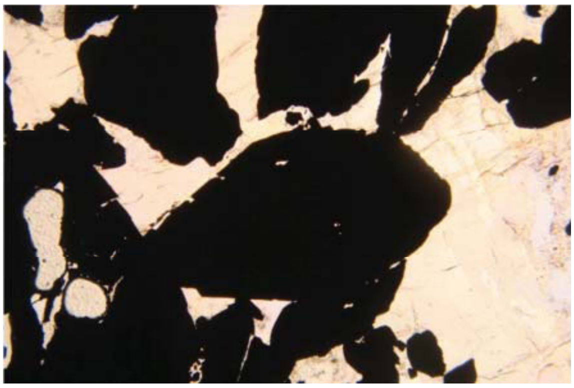

Figure 3-18: Braunite bedded in quartz in transmitted light (10 times extension, length of the picture correlates to 3.6 millimeters)

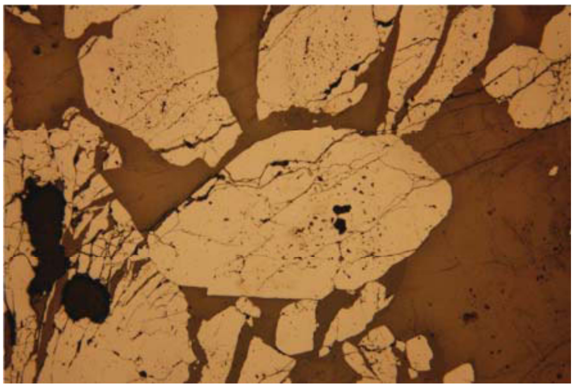

Figure 3-19: Braunite bedded in quartz in reflected light (10 times extension, length of the picture correlates to 3.6 millimeters)

Analysis	30	31	32
Mineralphase	*Braunite*	*Braunite*	*Braunite*
MgO	0,80	0,91	0,66
SiO_2	10,08	10,27	10,27
CaO	0,42	-	0,35
MnO	7,92	8,08	8,19
Mn_2O_3	79,46	80,82	80,47
FeO	2,07	2,47	2,35
Sum	**100,74**	**102,55**	**102,30**
Oxygen	12	12	12
Mg^{2+}	0,12	0,13	0,10

Analysis	30	31	32
Mineralphase	*Braunite*	*Braunite*	*Braunite*
Si^{4+}	1,00	1,00	1,00
$Ca^{2+rement}$	0,04	-	0,04
Mn^{2+}	0,67	0,67	0,68
Mn^{3+}	6,00	6,00	5,99
Fe^{2+}	0,17	0,20	0,19

Table 3-7: Scanning electron microscope analyses of Braunite from SM24 (Oxides are given in mass%, ionic composition is calculated according to 12 oxygen atoms in general mineral formulas. Total content of MnO and Mn_2O_3 are calculated according to the method of Droop 1987)

3.2.5. SM31

Sample SM31 can be described as a red to green/grey laminated rock with a high amount of quartz (figure 3-18). Grain size is about one millimeter. Layering of the minerals could be recognized. The green to grey phase is an epidote. In this phase very small dark green or black grains are observed with the loupe (ten times magnification). Macroscopically the red phase couldn't be identified.

The main minerals of this section are epidotes, as accessories minerals are mica, titanite – $CaTi(SiO_4)O$, hematite – Fe_2O_3 and feldspars with actinolite needles – $\{Ca_2\}\{(Mg,Fe^{2+})_5\}(Si_8O_{22})(OH)_2$. Quartz is building up the basic mass and has undulatory extinction, especially at rims, which is an indication for plastic deformation.

Figure 3-20: Scanned thin section SM31 (length of the picture correlates to 2.8 x 4.8cm)

The green to grey mentioned phase in the description of the rock sample, looks in the microscope green to brown, sometimes reddish. They are having very high colors of interferences, yellow in the one position and pink to violet in the other position. The grains have partially rounded boarders. These minerals show a clear-cut lamination and no regulation in the texture can be observed and can be identified as zoned epidotes (figure 3-21). The center is white surrounded of green discoloration and the boarders are red. A few relicts of hematite associated with epidotes have been observed.

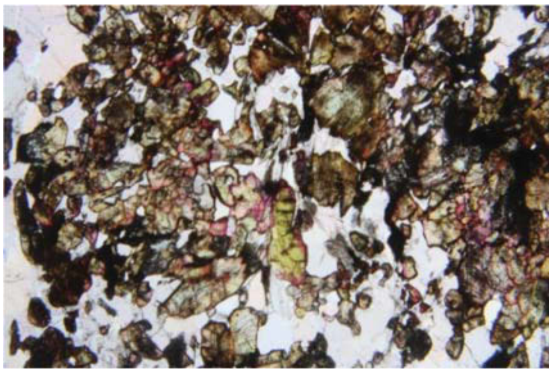

Figure 3-21: Quartz and epidotes in transmitted light (10 times extension, length of the picture correlates to 3.6 millimeters)

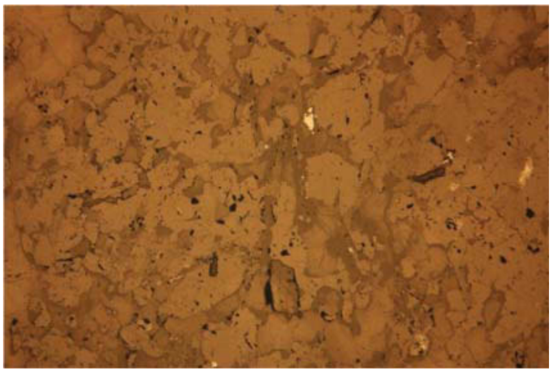

Figure 3-22: Quartz and epidotes in reflected light (10 times extension, length of the picture correlates to 3.6 millimeters)

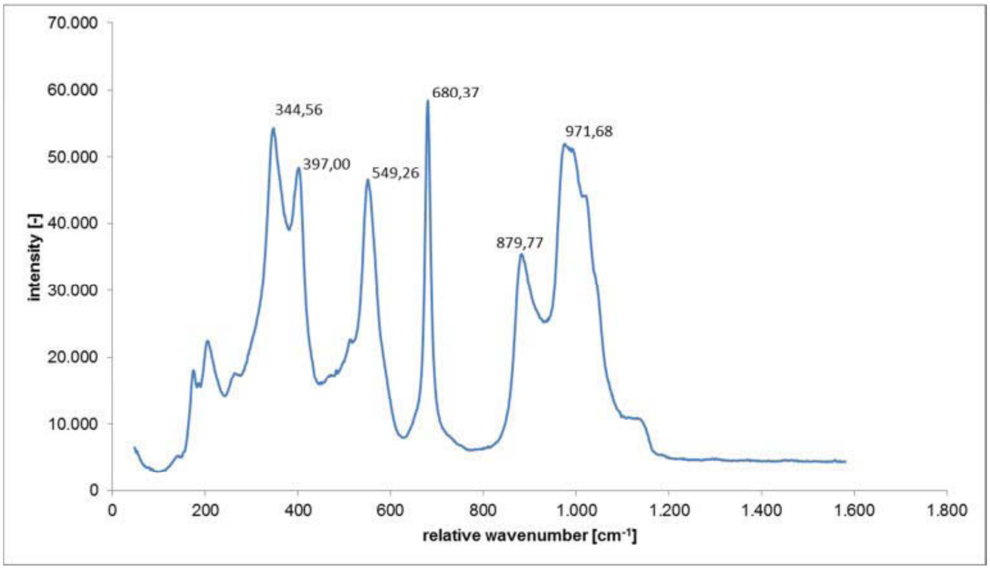

Diagram 3-1: Raman analysis of epidote and pyroxene, 680 cm^{-1} (sample SM31)

As it was mentioned, those small green to black minerals in the epidote dominated area could be measured via scanning electron microscope. The scanning electron microprobe analyses according to the aegirine-augite series. The strong intergrowth of clinopyroxenes and epidotes can also be seen in in diagram 3-1. These pyroxenes could be relicts of the high-pressure metamorphism.

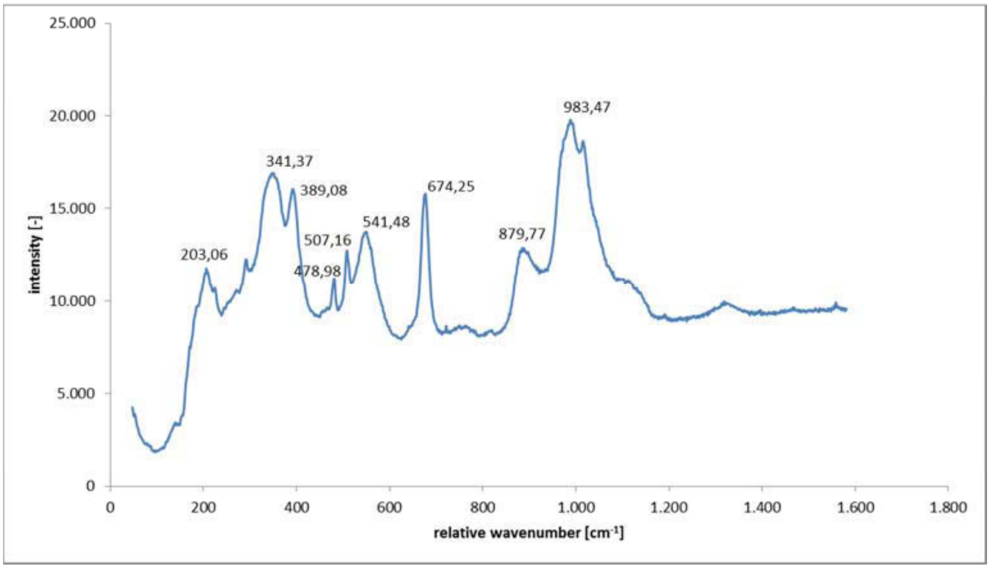

Diagram 3-2: Raman analysis of epidote and probably aegirine-augite, 680 cm^{-1} (sample SM31)

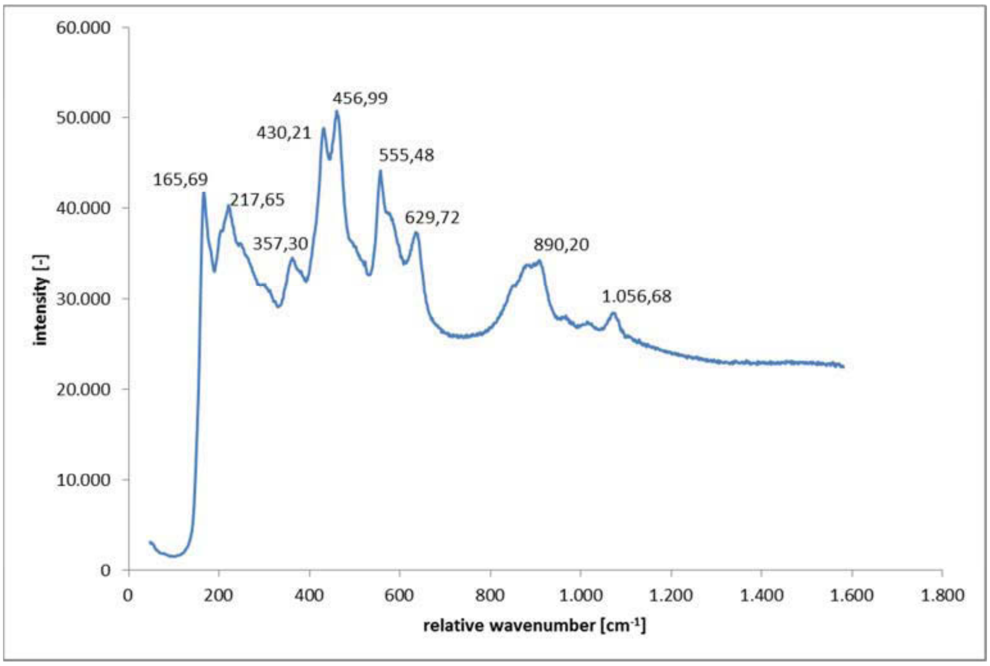

Diagram 3-3: Raman analysis of piemontite, 680 cm^{-1} (sample SM31)

Diagrams 3-1 to 3-3 illustrate the Raman spectra of some common minerals of this section. Some spectra illustrate interference between two minerals because the spot-size of the laser beam exceeded the size of the single mineral grain,

In table 3-8 are some characteristic epidote and augite analyses plotted.

Analysis	39	40	41	42
Mineralphase	*Epidote*	*Epidote*	*Augite*	*Augite*
Na_2O	-	-	8,43	7,09
MgO	-	-	8,21	9,02
Al_2O_3	22,90	22,50	5,82	4,29
SiO_2	39,10	39,15	57,16	56,47
CaO	24,07	23,70	11,10	13,03
MnO	1,54	0,98	-	-
FeO	12,66	13,34	11,75	11,30
Sum	**100,27**	**99,68**	**102,45**	**101,20**
Oxygen	12,5	12,5	6	6
Na^+	-	-	0,57	0,49
Mg^{2+}	-	-	0,43	0,48
Al^{3+}	2,08	2,06	0,24	0,18
Si^{4+}	3,01	3,04	2,00	2,01
Ca^{2+}	1,99	1,97	0,42	0,50
Mn^{2+}	0,10	0,06	-	-
Fe^{2+}	0,82	0,87	0,34	0,34

Table 3-8: Scanning electron microscope analyses of epidotes and augites from SM24

3.2.6. SM35

This is a complex section without any clear bands of compositional differences. The main minerals in this section are piemontite, calcite, braunite, quartz and feldspar. At the edge there is a large crystal of greenovite, a pink Mn-rich titanite. Additional, a needle-like amphibole is observed.

Figure 3-23: Scanned thin section SM35 (length of the picture correlates to 2.8 x 4.8cm)

Quartz, feldspar and braunite form a course-grained band-like structure, whereas in adjacent sectors a fine grained piemontite assemblage occurs in course-grained calcite.

As it can be seen in figure 3-23, there is a big pink grain assemblage at the bottom of the image. In the microscope (see figure 3-24 and 3-25) these minerals are brown and almost opaque. Scanning electron microscope analyses confirm the nature of this mineral: titanite. Especially it can be named as greenovite, a manganese rich variety of titanite. This mineral makes a very compact impression, with a pinkish pleochroism and high interference colors of fourth or fifth order.

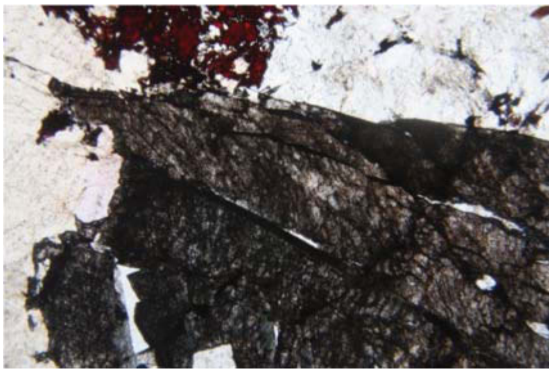

Figure 3-24: Greenovite in transmitted light (10 times extension, length of the picture correlates to 3.6 millimeters)

Figure 3-25: Greenovite in reflected light (10 times extension, length of the picture correlates to 3.6 millimeters)

Other mineral phases which could be observed are calcite, albite and braunites. The calcites occur next to the quartz. Calcite minerals are having a light pinkish color and with the scanning electron microscope analyses about five percent strontium could have been established. In the calcite dominated areas small piemontite grains with a very high content of wolfram could have been observed. Those bedded piemontites having a size between 20 – 65 µm (see figure 3-24) and their wolfram contents are about 13.74% (see table 3-9).

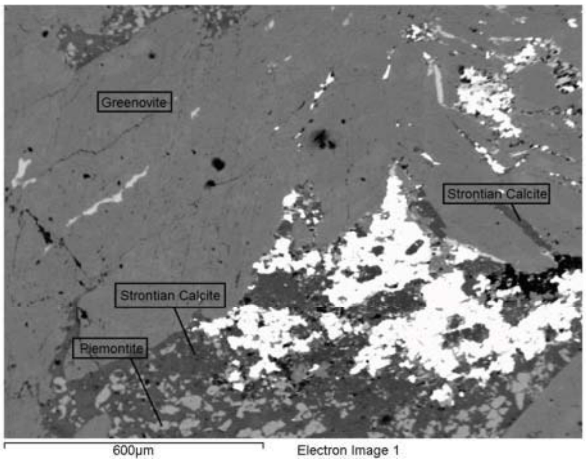

Figure 3-26: Electron image SM35.2, done during the measurements

The bright white mineral phase is probably hollandite based on preliminary microprobe analyses. Analysis number 52 of table 3-9 illustrates probably an allanite, which is variety of epidote that is rich in REE. In the microscope it looked similar to a piemontite, but scanning electron microscope analyses indicate similarities with allanite composition.

Analysis	46	47	48	50	51	52
Mineralphase	*Greenovite*	*Augite*	*Braunite*	*Strontian Calcite*	*Strontian Calcite*	*Allanite*
Na_2O	-	4,70	-	-	-	-
MgO	-	12,49	-	-	-	-
Al_2O_3	0,87	1,06	-	-	-	13,87
SiO_2	30,14	54,96	9,95	-	-	30,31
CaO	28,82	17,29	0,85	61,89	60,10	15,87
TiO_2	38,65	-	-	-	-	-
MnO	0,63	0,61	8,07	1,45	-	10,77
Mn_2O_3	-	-	79,26	-	-	7,61
FeO	-	8,88	2,62	-	-	4,90
SrO	-	-	-	4,45	5,65	-
SnO_2	-	-	-	-	1,56	-
WO_3	-	-	-	-	-	13,74
Sum	**99,12**	**99,98**	**100,76**	**67,78**	**67,31**	**97,07**
Oxygen	5	6	12	3	3	12,5
Na^+	-	0,33	-	-	-	-
Mg^{2+}	-	0,67	-	-	-	-
Al^{3+}	0,03	0,05	-	-	-	1,52
Si^{4+}	0,99	1,99	0,99	-	-	2,81
Ca^{2+}	1,01	0,67	0,09	0,95	0,94	1,58
Ti^{4+}	0,95	-	-	-	-	-
Mn^{2+}	0,02	0,02	0,68	0,02	-	0,85
Mn^{3+}	-	-	6,02	-	-	0,54
Fe^{2+}	-	0,27	0,22	-	-	0,38
Sr^{2+}	-	-	-	0,04	0,05	-
Sn^{4+}	-	-	-	-	0,01	-
W^{6+}	-	-	-	-	-	0,33

Table 3-9: Selected scanning electron microprobe analyses of SM35 (Oxides are given in mass%, ionic composition is calculated according to the number of oxygen atoms in general mineral formulas. Total content of MnO and Mn_2O_3 are calculated according to the method of Droop 1987)

The manganese content of the greenovite is very small. But no reference measurements would found in literature for comparison. The classification of greenovite was carried out with the comparison of the color in the hand piece. Because no other pink titanite than greenovite is known.

3.2.7. SM39

The hand piece contains a large mass of dark-burgundy colored minerals, which are identified as piemontite. Also big amount of quartz-rich fissures can be seen. Those fissures are more or less parallel to each other. At the surface of the sample a thin layer of white amphiboles can be seen.

Figure 3-27: Scanned thin section SM35 (length of the picture correlates to 2.8 x 4.8cm)

The thin section analyses confirmed the first description. The whole sample is built up by piemontites, a manganese rich variety of epidote. Amphiboles are also observed in the thin section (see figure 3-25 right handed white to translucent area). The amphiboles having a white to a bright blue color in the microscope. Their clear columnar habitus makes it easy to distinguish it from quartzes. Those white amphiboles are tremolites. They amphibole grains show no deformation and they are grown astral from different points more or less. The quartz veins contain many fluid inclusions and also small crystals piemontite (up to one millimeter) are included.

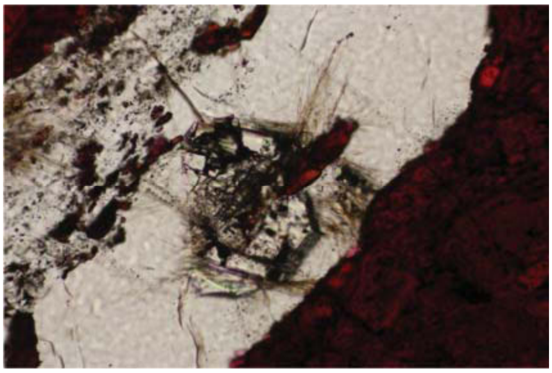

Figure 3-28: Piemontite inclusions in a quartz-rich fissure - transmitted light (10 times extension, length of the picture correlates to 3.6 millimeters)

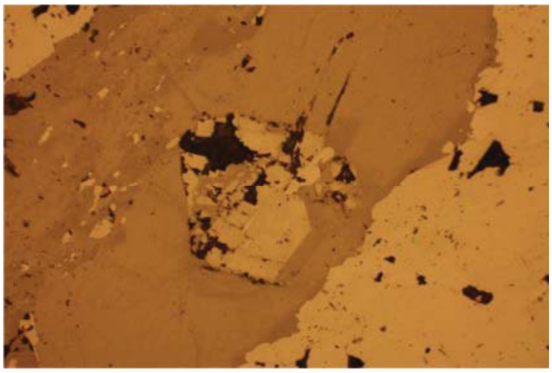

Figure 3-29: Piemontite inclusions in a quartz-rich fissure - reflected light (10 times extension, length of the picture correlates to 3.6 millimeters

In the fissures (see figure 3-28 and 3-29) also diopside and orthoclase are observed. But their total volume percentage in the fissures is less than five percent. Piemontite measurements with the aid of scanning electron microscope and microprobe are presented in table 3-10.

	54	55	56	58	59
Mineralphase	*Piemontite*	*Piemontite*	*Piemontite*	*Tremolite*	*Tremolite*
Na_2O	-	-	-	1,29	-
MgO	-	-	-	24,24	24,96
Al_2O_3	19,16	19,76	19,33	0,79	-
SiO_2	38,16	38,16	38,83	61,80	64,92
CaO	23,51	21,86	23,60	12,52	16,51
MnO	16,41	14,94	15,24	-	-
FeO	2,38	1,97	2,57	1,11	-
SrO	-	2,79	-	-	-
Sum	**99,62**	**99,48**	**99,57**	**101,76**	**106,39**
Oxygen	12,5	12,5	12,5	23	23
Na^+	-	-	-	0,33	-
Mg^{2+}	-	-	-	4,68	4,66
Al^{3+}	1,77	1,85	1,79	0,12	-
Si^{4+}	3,00	3,03	3,05	8,01	8,13
Ca^{2+}	1,98	1,86	1,98	1,74	2,21

	54	55	56	58	59
Mineralphase	*Piemontite*	*Piemontite*	*Piemontite*	*Tremolite*	*Tremolite*
Mn^{2+}	1,09	1,00	1,01	-	-
Fe^{2+}	0,16	0,13	0,17	0,12	-
Sr^{2+}	-	0,13	-	-	-

Table 3-10: Scanning electron microscope analyses of Piemontite and Tremolite of SM39

In contrast to the other piemontite analyses (see table 3-4 and 3-5) no wolfram could be detected, but measurement 55 (see table 3-10) shows the same amount of strontium instead of wolfram. Like the origin of wolfram, the origin of strontium is unknown. Tremolite analyses are unremarkable.

It was tried to test with Raman, if the orientation of the piemontite causes any differences in the Raman spectra (diagram 3-5). Both measurements were done under the same terms. In general are just differences of the intensity recognizable. The intensities of measurements parallel to the mineral orientation are about 20 to 25% stronger than those which are vertical to the mineral orientation. Two other peaks could be observed at the spectra's, which are too flimsy in the spectra's parallel to the orientation. First additional peak is at 198.20 cm^{-1} and the second peak plots at 500.91 cm^{-1} (see diagram 3-5).

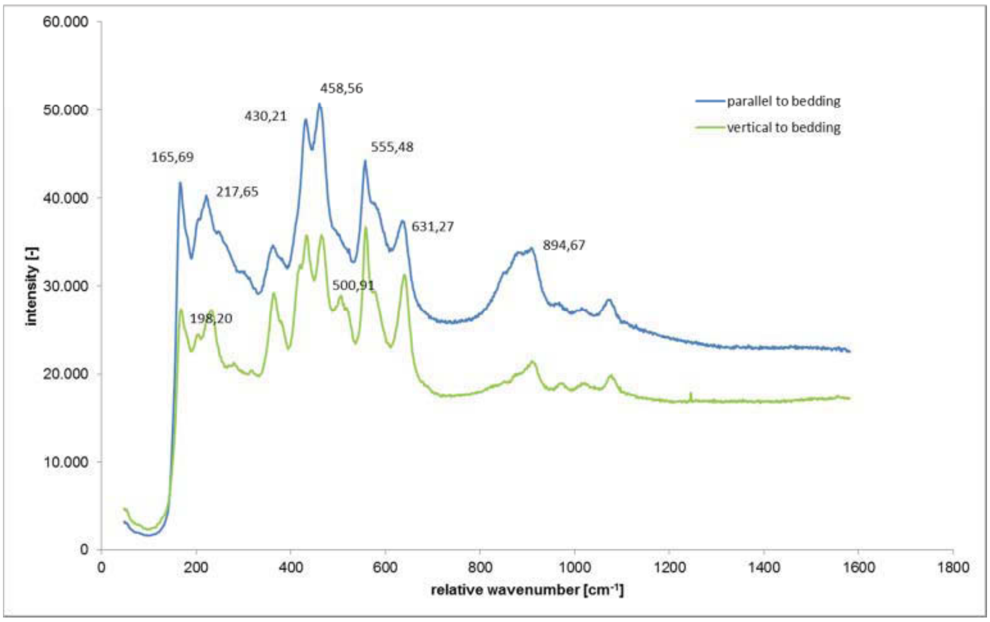

Diagram 3-4: Parallel and vertical Raman spectra of a piemontite mineral, 680 cm^{-1} (sample SM39)

Raman detected minerals are calcite, feldspar and a white mineral with a habitus of needles, probable tremolite (diagram 3-6).

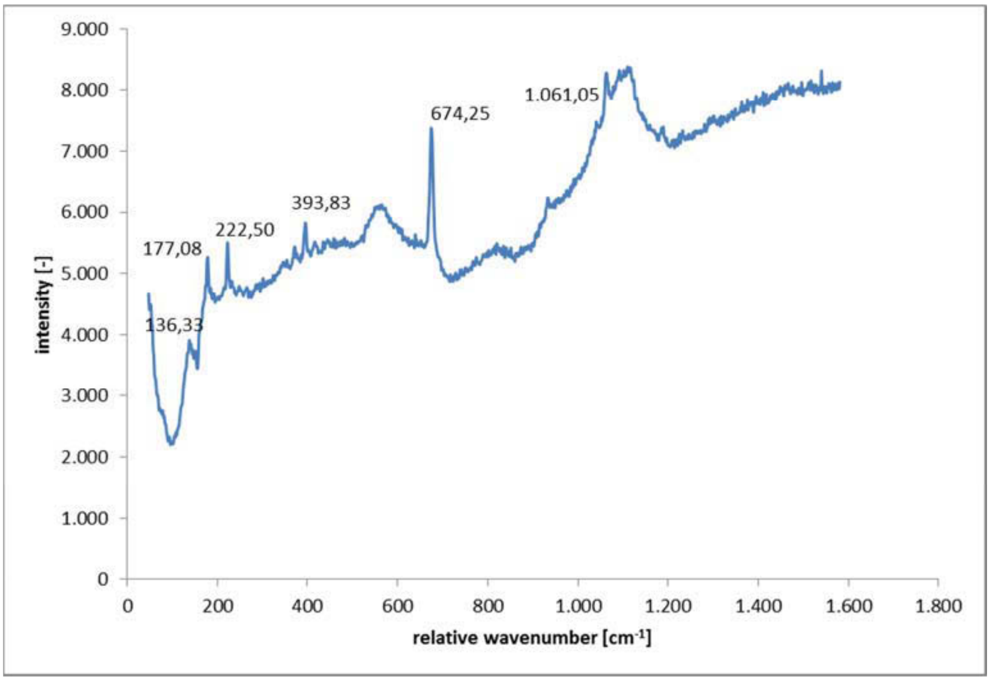

Diagram 3-5: Raman spectra of tremolite, 680 cm^{-1} (sample SM39)

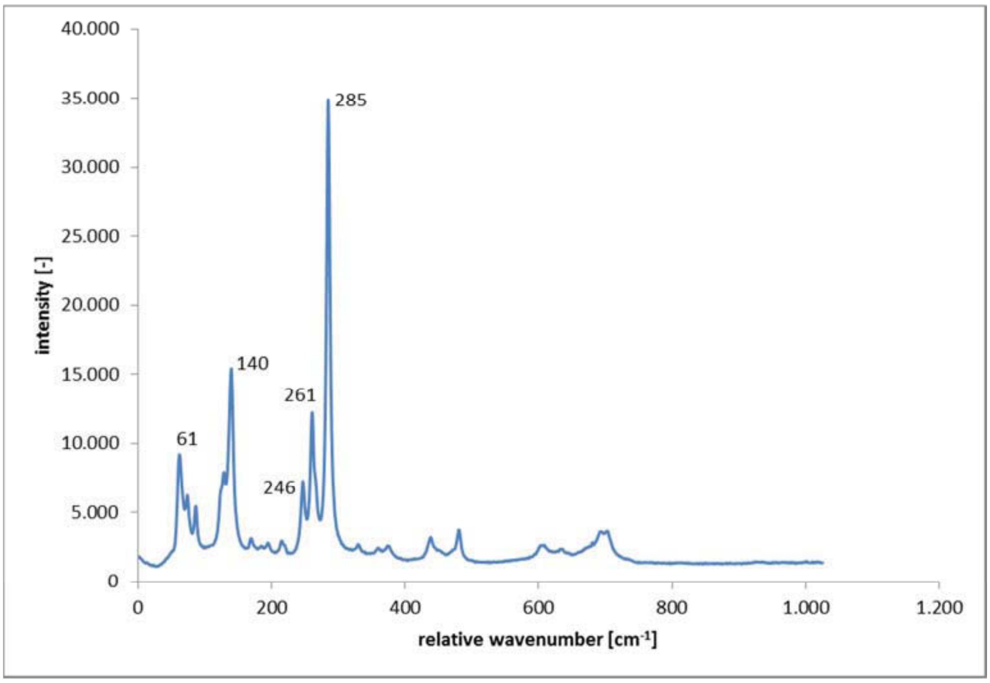

Diagram 3-6: Raman spectra of feldspar, 680 cm^{-1} (sample SM39)

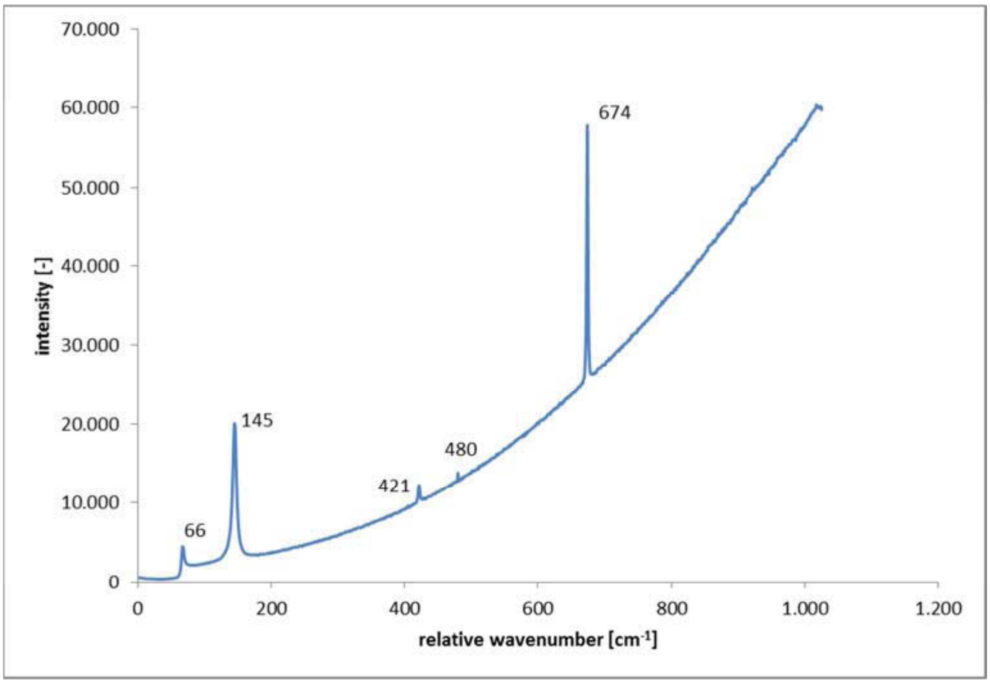

Diagram 3-7: Raman spectra of calcite, 680 cm^{-1} (sample SM39)

As mentioned before, a large number of fluid inclusions are present the quartzitic fissure (figures 3-30 to 3-31), which can be studied on composition and density. The compositions of the fluid inclusions were measured with Raman. The gas phases CO_2 and N_2 could be detected in all measured vapor bubbles of the fluid inclusions. However, the Raman signal is very weak, indication a low concentration. CH_4 was not detected. The fluid phase is made out of brines.

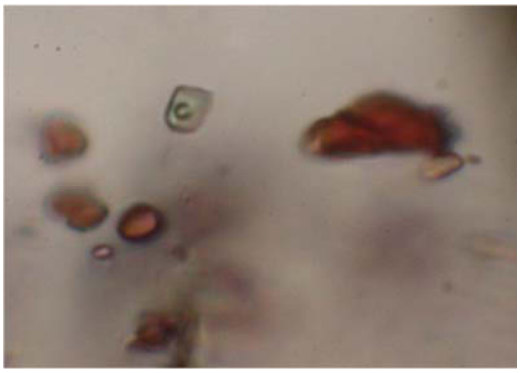

Figure 3-32: Fluid and piemontite inclusions of the quartzitic fissure (length of the picture correlates to 0.24 mm)

Figure 3-31: Fluid inclusion of the quartzitic fissure (length of the picture correlates to 0.18 mm)

Figure 3-30: Fluid inclusion of the quartzitic fissure (length of the picture correlates to 0.12 mm)

With the aid of microthermometry homogenization and melting temperature could be measured (table 3-11). The homogenization temperature of those inclusions ranges from 184.3℃ to 227.5℃ with a minimum outliner at 173.1℃ and a maximum outliner at 234 ℃. The mode of homogenization occurs between 190 and 200℃ (figure 3-3). The melting temperatures are much more homogeneous they vary from -5.6℃ up to -1.8℃. The mode of melting occurs between -4 and -3℃ (figure 3-4).

sample	**homogenization temperature [℃]**	**melting temperature [℃]**	**salinity [%]**[5]	**homogenization pressure [MPa]**[6]	**density [g/cc]**[6]
FI-1	173,1	-4,2	6,67	0,7017	0,9443
FI-2	203,4	-4,0	6,38	1,3609	0,9141
FI-3	184,8	-1,8	2,96	0,8984	0,9073
FI-4	215,2	-3,4	5,47	1,7658	0,8940
FI-5	186,8	-3,9	6,23	0,9387	0,9291
FI-6	194,4	-3,8	6,08	1,1120	0,9208
FI-7	201,7	-4,1	6,52	1,2896	0,9176
FI-8	205,0	-4,4	6,96	1,4104	0,9169
FI-9	196,7	-4,0	6,38	1,1709	0,9208
FI-10	202,3	-2,8	4,55	1,3278	0,9008
FI-11	193,8	-3,2	5,25	1,0971	0,9152
FI-12	205,6	-5,0	7,82	1,4294	0,9229
FI-13	191,8	-3,5	5,63	1,0491	0,9200
FI-14	211,6	-4,6	7,25	1,6323	0,9125
FI-15	209,7	-2,7	4,39	1,5654	0,8912
FI-16	190,9	-3,4	5,47	1,0282	0,9197
FI-17	192,0	-4,0	6,38	1,0538	0,9253
FI-18	227,5	-4,7	7,40	2,2928	0,8966
FI-19	207,9	-3,9	6,23	1,5043	0,9082
FI-20	194,6	-4,6	7,25	1,1170	0,9291
FI-21	213,5	-3,4	5,47	1,7017	0,8959
FI-22	199,4	-5,6	8,65	1,2441	0,9347
FI-23	198,5	-3,8	6,08	1,2192	0,9167

---

[5] Calculations after Hall et al. 1988

[6] Calculations after Zhang and Frantz 1987

sample	homogenization temperature [℃]	melting temperature [℃]	salinity [%][5]	homogenization pressure [MPa][6]	density [g/cc][6]
FI-24	184,3	-3,5	5,63	0,8886	0,9272
FI-25	187,5	-4,9	7,68	0,9533	0,9386
FI-26	189,1	-2,9	4,70	0,9878	0,9159
FI-27	234,0	-4,6	7,25	2,3627	0,8878
FI-28	216,3	-3,3	5,32	1,8085	0,8915
FI-29	220,1	-3,7	5,93	1,9623	0,8923
FI-30	217,3	-4,6	7,25	1,8479	0,9065

Table 3-11: Homogenization and melting temperatures of measured fluid inclusions, with calculated salinity, homogenization pressure and density

All analyses illustrate melting temperatures higher than -21.2℃. So it can be assumes, that the fluid phase of all inclusions in this sample, is a mixture of NaCl and H_2O. Via the software program AqSo2e *[Bakker 2003]*, the salinity was calculated. Generally the salinity ranges from 4.39% up to 7.68% with two outliners.

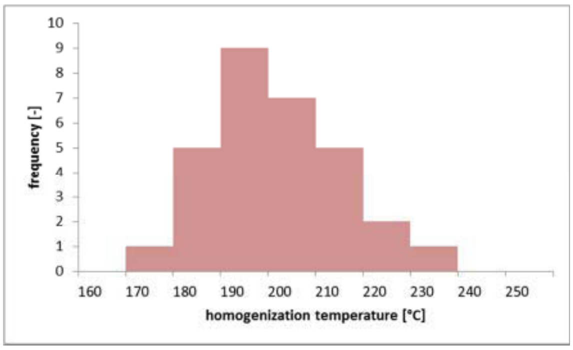

Diagram 3-8: Histogram of the homogenization temperature of the fluid inclusions in SM39 (30 values)

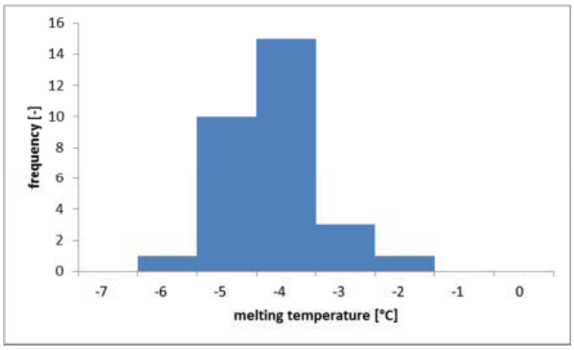

Diagram 3-9: Histogram of the melting temperature of the fluid inclusions in SM39 (30 values)

For the density calculations the program Loner 38 *[Bakker 2003]* was used, on the basis of the formula by Zhang and Frantz (1987). The calculation method use homogenization temperature to calculate densities. Those calculated densities ranging from 0.8878 g/cc up to 0.9443 g/cc.

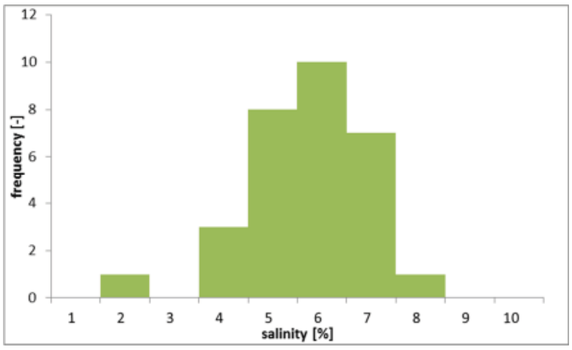

Diagram 3-10: Histogram of salinity of the fluid inclusions in SM39 (30 values)

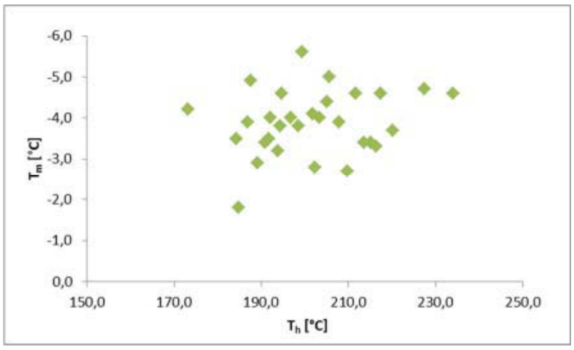

Diagram 3-11: Homogenization temperature vs. Melting temperature of the fluid inclusions in SM39 (30 values)

As it can be seen in diagram 3-9 and 3-10 about 50% of all measurements fitting in the same range. The field of the melting temperature is even much closer than the field of homogenization temperatures. The same observation can be done in diagram 3-11.

These analyses illustrate that the fluid trapped in quartz fissures is homogeneous, and represent a high density aqueous fluid with small amounts of salt, CO_2 and N_2.

3.2.8. SM42

Sample SM42 is from the Servette mine. It is rich in garnet with sizes up to one centimeter in diameter. The matrix of the garnet grains is probably a compact mass made out of quartz, smaller garnet grains with some pyrites and micas. The hand specimen has a relative high density, due to the large amount of garnet in the sample. The garnet grains are dark red and the matrix is orange colored.

Figure 3-33: Scanned thin section of SM42 (length of the picture correlates to 2.8 x 4.8cm)

The macroscopically determined mineral assemblage is confirmed by optical microscopy analyses. The whole sample is build up by garnets, more specific almandine. Grain boarders are perfectly defined, some grains are brittle deformed and the fissures are filled up with garnet-rich material again. The grain size varies from one millimeter up to two centimeters. Accessories minerals are rutile, pyrite, bronzite and orthopyroxene.

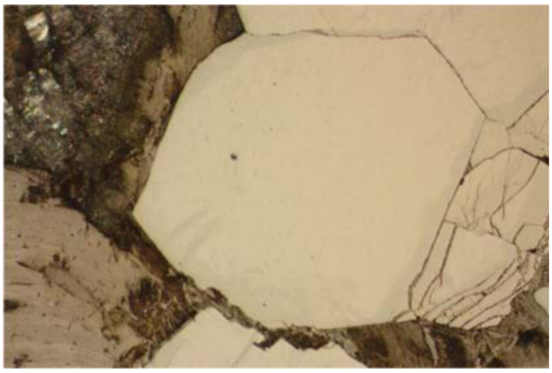

Figure 3-34: Almandine - reflected light (10 times extension, length of the picture correlates to 3.6 millimeters)

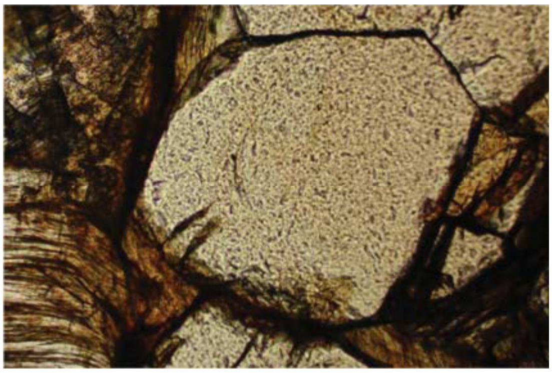

Figure 3-35: Almandine - transmitted light (10 times extension, length of the picture correlates to 3.6 millimeters)

In figure 3-29 an almandine with an extension about 1.8 centimeters can be seen. The enstatite is much better recognizable in figure 3-30. It's the brown to white laminated mineral left sided of the almandine. The occurrence of this mineral is less than one percent of the whole sample.

The microprobe analyses of almandine show small amounts of sulfur, vanadium and chrome. The measurements 63 and 65 (see table 3-13) were in the same garnet grain. It was a kind of trial to test variation in chemistry between rim and core of garnet crystals. Analysis 63 is performed near the center and analysis 65 is performed next to the boarder. Small variations of potassium calcium and the ratio of FeO to Fe_2O_3 can be observed. The content of potassium and calcium increases from the center to the rims. Potassium content increases from the center to the boarder more than 2.5 times, calcium increases about ten percent. The ratio from FeO to Fe_2O_3 decreases from the center to the boarder from 3.8118 at the center to 3.1911 at the rim. The guesswork of a garnet zoning could be detected.

	61	63	65	73
Mineralphase	*Almandine*	*Almandine*	*Almandine*	*Enstatite*
Na_2O	0,06	0,02	0,01	0,01
MgO	3,86	4,85	4,99	33,03
Al_2O_3	16,66	17,36	17,28	0,09
SiO_2	35,50	35,42	35,04	59,21
SO_3	0,02	-	0,02	-
K_2O	0,09	0,19	0,50	0,36

	61	63	65	73
Mineralphase	*Almandine*	*Almandine*	*Almandine*	*Enstatite*
CaO	1,22	0,99	1,10	0,02
TiO_2	0,04	0,03	0,02	-
V_2O_3	0,01	-	-	-
Cr_2O_3	-	-	0,00	-
MnO	0,02	0,01	0,02	0,00
FeO	33,56	31,79	30,06	5,77
Fe_2O_3	7,34	8,34	9,42	-
Sum	**98,36**	**99,00**	**98,48**	**98,48**
Oxygen	24	24	24	3
Na^+	0,02	0,01	0,00	0,00
Mg^{2+}	0,96	1,19	1,23	0,86
Al^{3+}	3,27	3,36	3,36	0,00
Si^{4+}	5,91	5,82	5,78	1,04
S^{6+}	0,00	0,00	0,00	-
K^+	0,02	0,04	0,11	0,01
Ca^{2+}	0,22	0,17	0,19	0,00
Ti^{4+}	0,00	0,00	0,00	-
V^{3+}	0,00	-	-	-
Cr^{3+}	-	-	0,00	-
Mn^{2+}	0,00	0,00	0,00	0,00
Fe^{2+}	4,67	4,37	4,15	0,08
Fe^{3+}	0,92	1,03	1,17	-

Table 3-12: Selected microprobe analyses of almandine and enstatite - SM42 (Oxides are given in mass%, ionic composition is calculated according to 24 oxygen atoms. Total content of FeO and Fe_2O_3 are calculated according to the method of Droop 1987)

Analysis	61	63	65
Almandine	88,92	87,29	86,58
Spessartine	0,03	0,02	0,05
Pyrope	8,39	10,55	10,95
Grossular	2,65	2,15	2,42

Table 3-13: Calculations of end members of measured garnets from table 3-12, in percentages

The calculations of the garnet end member yielded more than 85 % almandine and about 10 % Pyrope (see table 3-13).

The garnet and quartz contain many types of inclusions, e.g. solid and liquid phases. In the quartz rich areas fluid inclusions were studied with the microthermometry and Raman spectroscopy. Some garnets contain isolated solid quartz inclusions. The Raman analyses (see diagram 3-7) of those quartz grains are showing a clear peak shifts in the main peak position (466 cm^{-1} at room conditions). These peak shifts are resulting from the entrapment of quartz during high pressure metamorphic conditions in garnets that act as rigid containers, and therefore preserve the highly pressurized quartz grains. The main peak of quartzes is 464 cm^{-1} according to Schmidt and Ziemann (2000) The measurements of the quartz in this study reveal peak positions between 465.53 cm^{-1} and 471.81 cm^{-1}.

In comparison with the study of Schmidt and Ziemann (2000) quartz spectra with a peak shift of 7.81 cm^{-1} relative wavenumbers correspond to an internal pressure of 0.85 GPa. The other three peaks at 465.53 cm^{-1} are fixed in the Garnet with a pressure of 0.1 GPa.

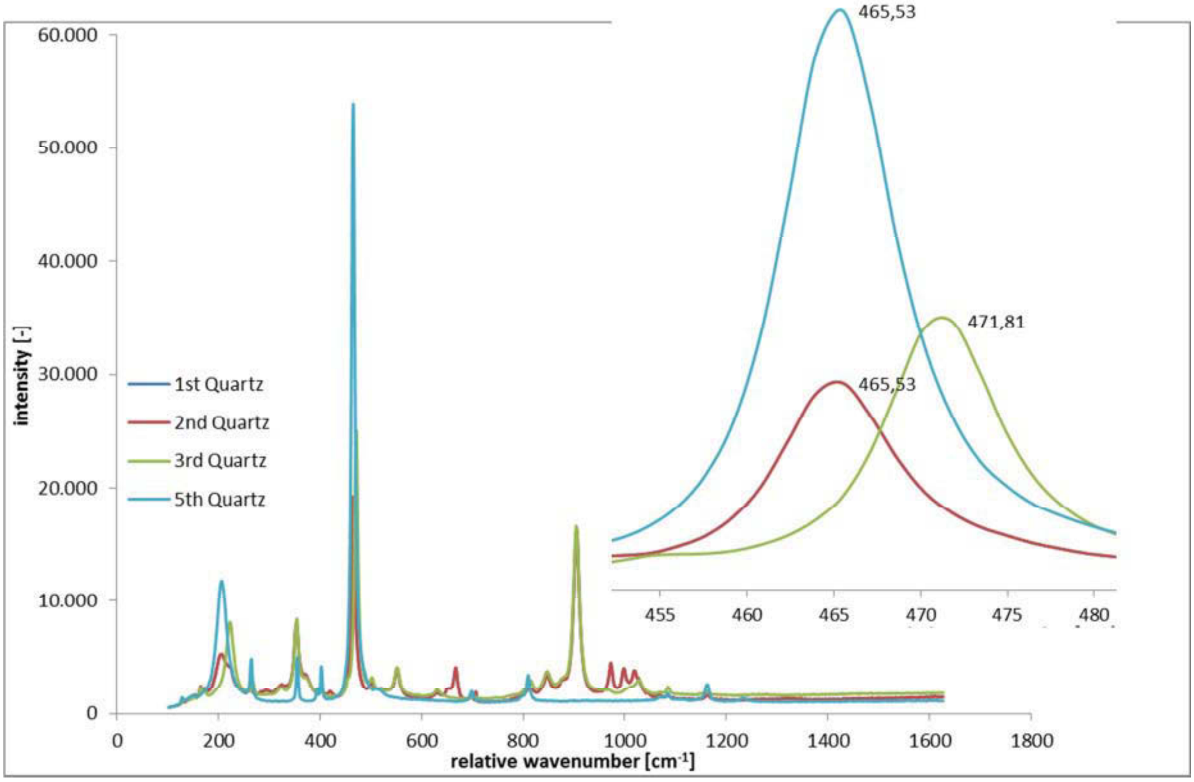

Diagram 3-12: High pressure Quartzes captured in Garnet (SM42)

The compositions of the fluid inclusions in quartz were measured with Raman spectroscopy. Only CO_2 was detected in all measured vapor bubbles of the fluid inclusions. Some vapor bubbles have minimal contents of N_2. Like in sample SM39 the amount of CO_2 and N_2 is very low and CH_4 was not detected. The liquid phase is brine.

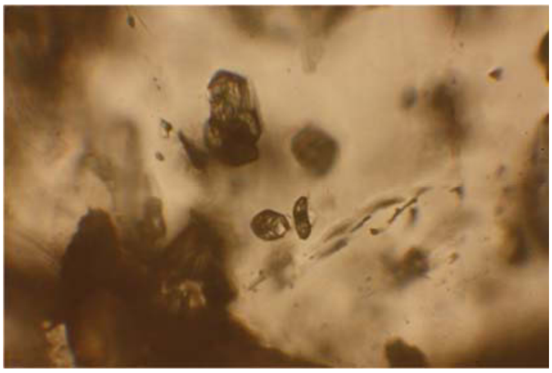

Figure 3-36: Quartz inclusions in garnets (length of the picture correlates to 0.65 mm)

Figure 3-37: Vapor inclusion in quartz, internal wall of the inclusion seemed to be graphitized (length of the picture correlates to 0.65 mm)

With microthermometry homogenization and melting temperature was measured (table 3-14). The homogenization temperature of these inclusions ranges from 193.7°C to 274.6°C, the results are widespread. The mode of homogenization occurs between 240 and 260°C (diagram 3-8). The melting temperatures vary from -7.7°C up to -1.7°C. The mode of melting occurs between -4 and -5°C (diagram 3-8).

sample	homogenization temperature [°C]	melting temperature [°C]	salinity [%][7]	homogenization pressure [MPa][8]	density [g/cc][8]
FI-1	239,8	-4,9	7,68	2,9375	0,8849
FI-2	205,4	-4,8	7,54	1,4230	0,9209
FI-3	274,6	not identified	-	-	-
FI-4	193,7	-7,5	11,11	1,0947	0,9568
FI-5	241,8	-1,7	2,80	3,0542	0,8338
FI-6	249,6	-6,0	9,19	3,5428	0,8873

---

[7] Calculation after Hall et al. 1988

[8] Calculation after Zhang and Frantz 1989

sample	homogenization temperature [℃]	melting temperature [℃]	salinity [%][7]	homogenization pressure [MPa][8]	density [g/cc][8]
FI-7	273,6	-5,2	8,10	5,4058	0,8457
FI-8	254,8	-7,7	11,35	3,8992	0,9009
FI-9	229,7	-4,1	6,52	2,3991	0,8863
FI-10	237,0	-4,6	7,25	2,7798	0,8843
FI-11	255,7	-4,0	6,38	3,9634	0,8519
FI-12	218,2	-4,4	6,96	1,8841	0,9031
FI-13	207,6	-4,8	7,54	1,4944	0,9188

Table 3-14: Homogenization and melting temperatures of measured fluid inclusions in quartz, with calculated salinity, homogenization pressure and density

For the calculations of the salinity it is assumed that NaCL is the main type of salt in the system, similar to sample SM39. For the calculations of the salinity the software program AqSo1e was chosen *[Bakker, 2003]*. The salinity ranges from 2.8% up to 11.4%.

As it can be seen in table 3-14, fluid inclusion number FI-3 has no melting temperature, because the transition from solid phase to liquid phase couldn't be fixed. So no calculations for salinity and density could have been performed for this inclusion.

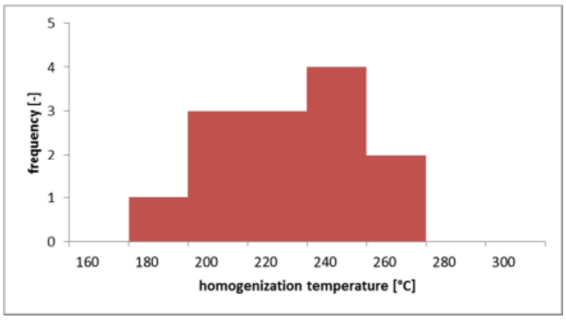

Diagram 3-13: Histogram of homogenization temperatures of the fluid inclusions in SM42 (13 values)

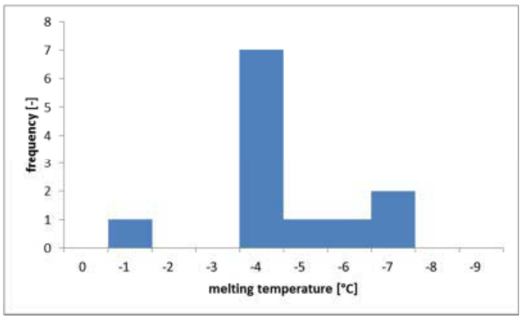

Diagram 3-14: Histogram of melting temperatures of the fluid inclusions in SM42 (13 values)

For the density calculations the program Loner 38 was used, on the basis of the formula by Zhang and Frantz (1987). The calculation follows with the homogenization temperature and the calculated density. Those calculated densities ranging from 0.8338 g/cc up to 0.9568 g/cc.

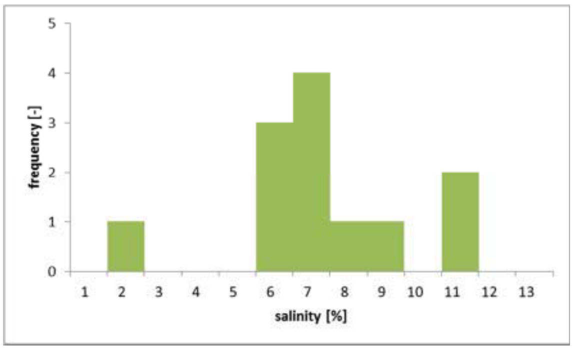

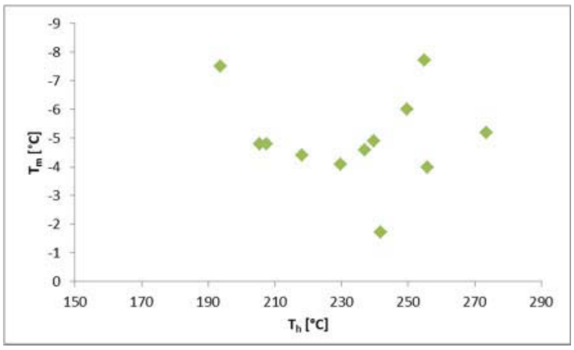

Diagram 3-15: Histogram of salinity of the fluid inclusions in SM42 (13 values)

Diagram 3-16: Homogenization temperatures vs. Melting temperatures in SM42 (13 values)

Homogenization temperatures of sample SM 39 from Prabornaz are lower than in sample SM 42 from Servette. The composition of the fluid inclusions in both localities is similar, mainly H_2O with about 4 mass% NaCl and minor amounts of CO_2 and N_2.

The difference in homogenization temperatures reflects the differences in density at both localities. Higher densities occur in the sample from Prabornaz, which may imply formation conditions at higher pressures or lower temperatures than the sample from Servette. Because high pressures could be identified in the Servette sample from Raman shift of the main peak of quartz, it can be assumed that the sample from Prabornaz was formed at relative lower temperatures.

3.2.9. SM48

The hand piece SM48 from Servette mine can be classified as blueschist with a clear foliation. Brown and turquoise secondary mineralizations are covering the sample. The brown spots are probably alterations of iron-rich sulfides (such as pyrite), whereas the turquoise spots are alterations of copper-rich sulfides (such as chalcopyrite).

Figure 3-38: Scanned thin section SM48 (length of the picture correlates to 2.8 x 4.8cm)

The main mineral phases in this sample are blue amphiboles (glaucophane), colorless micas and chlorite. These amphiboles are typically for high pressure metamorphism of basalts. The chlorite is overprinting the glaucophane, and is therefore formed in a later metamorphic stage than the high pressure metamorphism

The opaque phases are building up by magnetite, a few braunite grains and chalcopyrite and made a percentage less than two. Other minerals which occur in this sample are rutiles, zircons and titanites; they also occur just as secondary minerals, so their total amount is probably less than two percent. The thin section contains two carbonate-rich layers, which may represent original variation in lithologies (see figure 3-39).

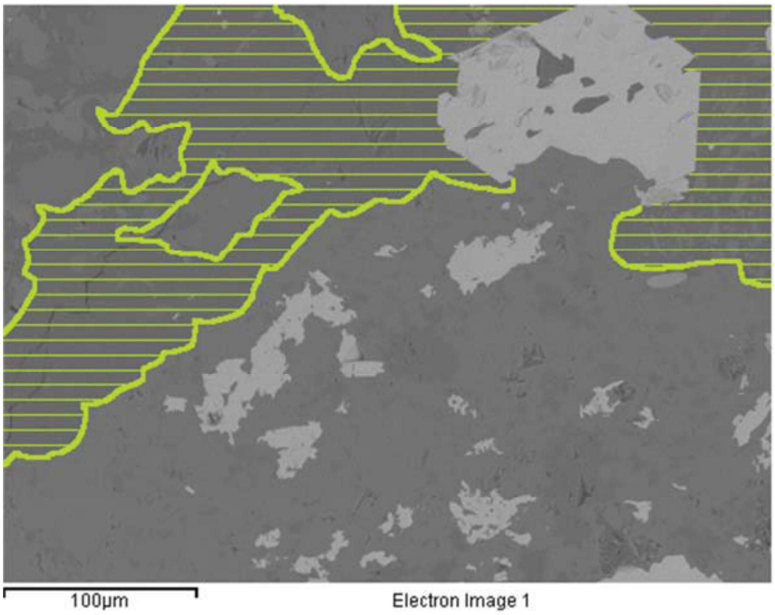

Figure 3-39: Scanning electron microscope picture of SM48 (ruled area illustrates albite)

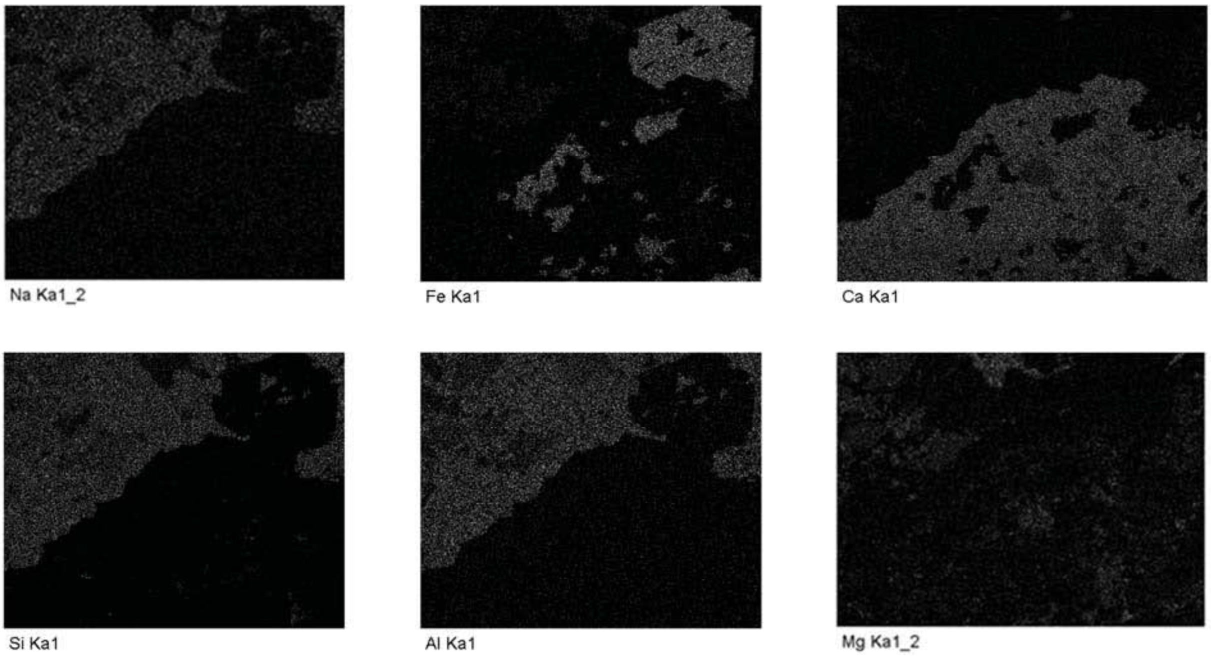

Figure 3-40: Landscaping of figure 3-39 – scanning electron microprobe (length of the single figures correlates to 400 µm - Ka in images complies with Kα)

The ruled area in figure 3-39 is albite which is intergrown with a calcite and dolomite domained area. In the carbonatic field some very fine grained hematites can be seen. Even figure 3-33 illustrates the boarder of albite to the carbonates much better. One of these dolomite grains has a size approximately to 70 µm. Those small dolomites can be seen as dark grey spots in the calcium landscaping of figure 3-40.

	89	90	91
Mineralphase	*Muscovite*	*Muscovite*	*Muscovite*
Na_2O	0,94	0,54	-
MgO	3,02	3,05	3,20
Al_2O_3	27,87	28,51	26,83
SiO_2	50,89	53,29	51,28
K_2O	11,40	11,32	10,34
FeO	2,93	3,58	2,60
ZnO	-	-	0,25
Sum	**97,05**	**100,29**	**94,49**
Oxygen	15	15	15
Na^+	0,12	0,07	-
Mg^{2+}	0,29	0,29	0,32
Al^{3+}	2,15	2,14	2,14
Si^{4+}	3,33	3,39	3,48
K^+	0,95	0,92	0,89
Fe^{2+}	0,16	0,19	0,15
Zn^{2+}	-	-	0,01

Table 3-15: Scanning electron microscope analyses of muscovites

Also Raman measurements were done and selected mineral phases are illustrated in the diagrams 3-17 and 3-18.

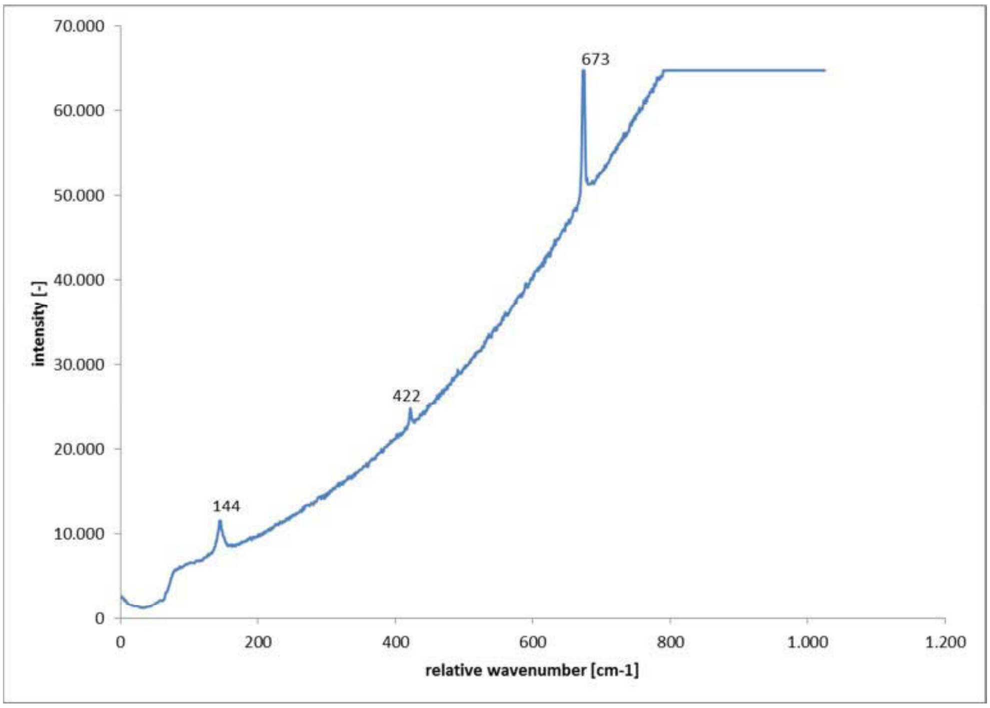

Diagram 3-17: Raman spectra of calcite, 680 cm^{-1} (sample SM42)

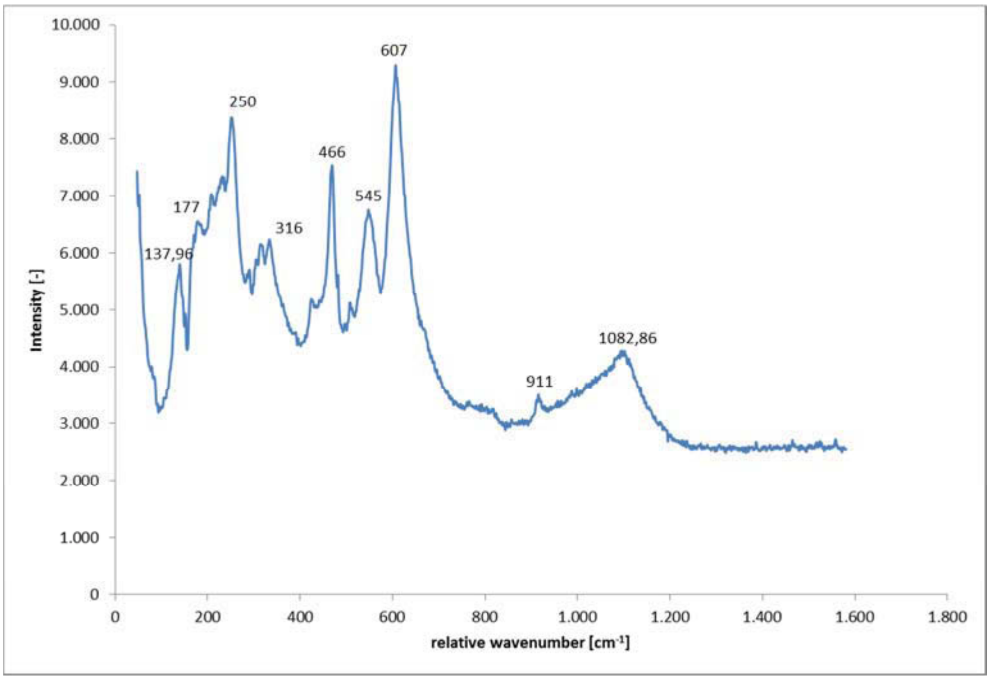

Diagram 3-18: Raman spectra of glaucophane, 680 cm^{-1} (sample SM42)

3.2.10. SM49

The hand piece can be dived in two different types of rock. One part is characterized by quartz and epidotes (see figure 3-41) and the other part is dominated by a greenish mass of minerals, mainly composed of short-needle amphiboles and light-green colored epidotes (see figure 3-41).

Figure 3-41: Scanned thin section SM49 (length of the picture correlates to 2.8 x 4.8cm)

The bright part of the sample (see figure 3-41) is build up by quartzes. This quartzitic massive is nerved by epidotes. It seemed so, that larger epidote minerals are parallel to each other. The smaller epidote grains occur as needles without orientation in the quartzitic area. Also a few actinolite needles could be observed. Some epidotes show pink colors of pleochroism the others are having a greenish pleochroism. In the big epidote grains are sometimes quartzes of 0.2 millimeters bedded. In figure 3-42 a big epidote with an actinolite needle is illustrated.

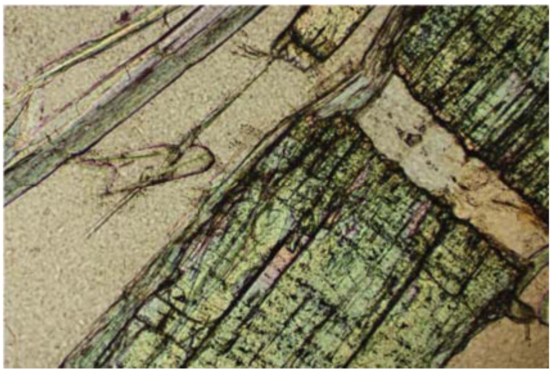

Figure 3-42: Epidote - transmitted light (10 times extension, length of the picture correlates to 3.6 millimeters)

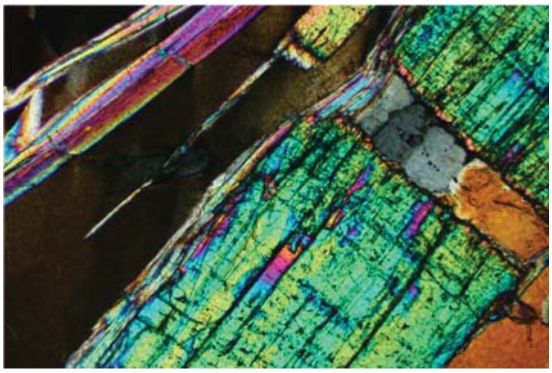

Figure 3-43: Epidote - transmitted light, crossed Nicol's (10 times extension, length of the picture correlates to 3.6 millimeters)

In the transition zone, from the quartzitic massive to the epidote and amphibole rich area, the epidotes getting rapidly smaller in comparison to those of the quartzitic union. They are showing a zoning in their colors.

The other part of the sample looks totally different (compare figures 3-42/43 with figures 3-44/45). The tremolites are much smaller and bedded without orientation in the sample. The Epidotes are in comparison to the tremolites much bigger and they are building up the main mineral phase of this part from the sample. Even by inspection of epidotes no orientation can be seen. The amphiboles can be named as tremolites and actinolite. The main mass is actinolite. They are showing a lot of different colors of interference. A bright pleochroism could be observed and they are showing a light green color in the microscope, and a light yellow to ocher color in the tool holder. In this part of the sample also a lot of fluid inclusions could be seen, as well in the amphiboles as in the quartzes.

Tremolites can be distinguished in figure 3-44 as the white to yellow looking columns, which show a variety of different colors with crossed Nicol's (see figure 3-45). In difference to the Tremolites of the other part of the sample they are much smaller. Even no chemical difference of both parts of the sample can be recognized. As secondary minerals can be named a few small garnet grains in the amphibole and epidote rich area.

Figure 3-44: Tremolites and epidotes - transmitted light (10 times extension, length of the picture correlates to 3.6 millimeters)

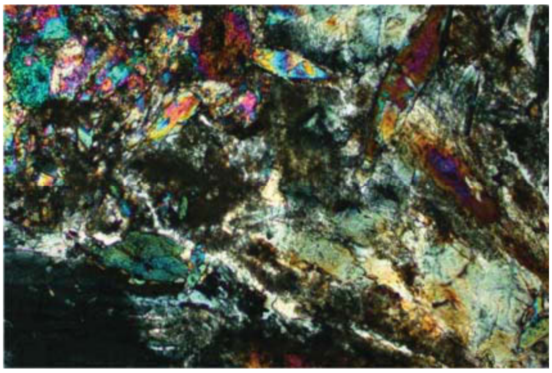

Figure 3-45: Tremolites and epidotes - transmitted light, crossed Nicol's (10 times extension, length of the picture correlates to 3.6 millimeters)

Analysis	103	104	106	107
Mineralphase	*Grossular*	*Almandine*	*Augite*	*Tremolite*
Na_2O	-	-	4,84	1,52
MgO	-	2,69	12,12	18,14
Al_2O_3	25,70	20,78	6,63	3,34
SiO_2	38,53	38,16	54,98	56,03
CaO	23,34	9,88	12,58	11,12
MnO	-	2,84	-	-
FeO	10,34	25,31	8,38	10,23
Fe_2O_3	-	2,37	-	-
Sum	**97,91**	**102,03**	**99,52**	**100,39**
Oxygen	24	24	6	24
Na^+	-	-	0,34	0,40
Mg^{2+}	-	0,62	0,65	3,67
Al^{3+}	4,73	3,82	0,28	0,54
Si^{4+}	6,02	5,95	1,99	7,61
Ca^{2+}	3,90	1,65	0,49	1,62
Mn^{2+}	-	0,38	-	-
Fe^{2+}	1,35	3,30	0,25	1,16
Fe^{3+}	-	0,28	-	-

Table 3-16: Selected scanning electron microscope analyses of SM49 (Oxides are given in mass%, ionic composition is calculated according to the number of oxygen atoms in general mineral formulas. Total content of FeO and Fe_2O_3 are calculated according to the method of Droop 1987)

As secondary mineral phases can be mentioned Grossular and Augite. Both minerals just have been observed in the Epidote rich part of the sample. Content of Augit is about ten percent, Grossulars appearance is much lesser.

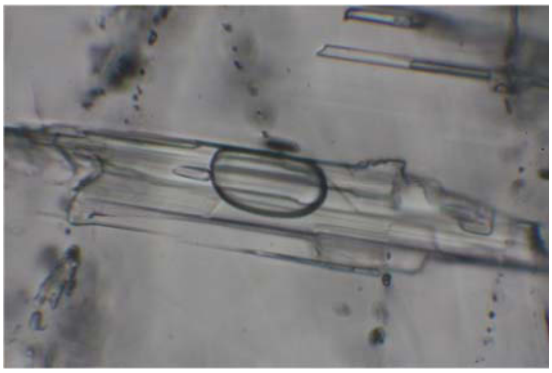

Figure 3-46: Large fluid inclusion trapped in an amphibole (length of the picture correlates to 0.8 mm)

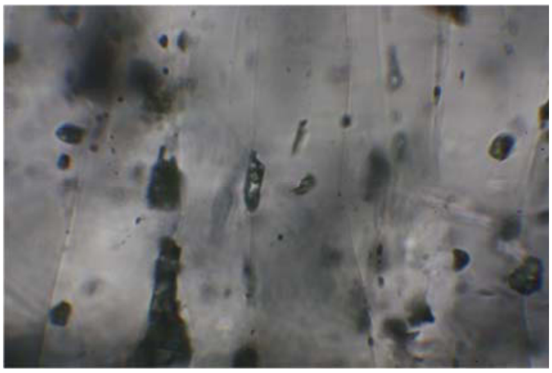

Figure 3-48: Fluid inclusion trapped in different depths in quartz (length of the picture correlates to 0.8 mm)

Figure 3-47: Fluid inclusion trapped in an amphibole (length of the picture correlates to 0.8 mm)

In the Quartz rich part of the sample a few fluid inclusions could have been observed. Even the bolds of the Tremolites are occurring fluid inclusions. Pervious Raman studies of the composition of those fluid inclusions, showed the existence of CO_2 and sometimes a very low content of N_2 in the bubble. All analyses of the fluid phase are showing very contents of salinity. The concentration of CO_2 and N_2 is to less for compositional calculations. The guesswork for this system was the same like the fluid inclusions of SM39 and SM42.

sample	**homogenization temperature [°C]**	**melting temperature [°C]**	**salinity [%][9]**	**homogenization pressure [MPa][10]**	**density [g/cc][10]**
FI-1	129,3	-15,9	19,36	0,4489	1,0667
FI-2	151,3	-10,3	14,27	0,4983	1,0086
FI-3	165,8	-18,5	21,32	0,6134	1,0515
FI-4	186,0	-22,7	24,11	0,9223	1,0568
FI-5	188,1	-16,9	20,13	0,9661	1,0218
FI-6	179,2	-16,6	19,91	0,7965	1,0278
FI-7	176,4	-17,3	20,44	0,7514	1,0344
FI-8	171,4	-17,2	20,36	0,6801	1,0381
FI-9	175,2	-16,3	19,67	0,7332	1,0293

Table 3-17: Homogenization and melting temperatures of measured fluid inclusions, with calculated salinity, homogenization pressure and density

The amount of fluid inclusion measurements with the microthermometry is too less for doing real interpretations. Causations therefore are two reasons. The most of the fluid inclusion in the Quartz mass have been too small for the observation of the phase transitions. The other reason is, those bubbles which could be seen in the Tremolites have been too close to the surface. The most of them got fissures during the heating or cooling phase.

Those analyzed fluid inclusions give a hint about the whole system. The homogenization temperatures are showing a very widespread range, with a minimum at 129.3° and a maximum at 188.1°C. The same observation can be done with the melting temperatures. But the values of the melting temperature approve the first guessed impression at the Raman measurement and the calculations attest the high salinity content, they are ranging from 14.27% up to 21.32%.

---

[9] Calculation after Hall et al. 1988

[10] Calculation after Zhang and Frantz 1989

4. Conclusion and discussion

In the course of this thesis, different rock samples of the manganese deposit at the Aosta Valley have been analyzed. The manganese deposit Prabornaz is biggest known manganese deposit of the western Alps. The ore body extends over 100m with a thickness from 0.4 to 8m thickness. Since several years the mining is abounded the main mined ore was braunite.

A lot of different manganese minerals could be observed and also a lot of minerals, which are normally no manganese bearing and due to the total mineral assemblages and the high pressure metamorphism, manganese integrated in their crystal lattice:

- Silicates
    - Phylosilicates:
        - Alurgite, variety of muscovite (contents less than 2.14 weight percent)
        - Aluminoceladonite, member of the mica group (about 2.09 wt%, just could be observed in the clinopyroxene domained areas)
    - Inosilicates:
        - Aeginerine-augite, member of the pyroxene group (less than 0.42 weight percent manganese)
        - Diopside, a clinopyroxene (manganese contaminations between 0.46 – 0.79 wt %)
        - Bronzite, variety of Enstatite a member of the orthopyroxene group (a maximum of 0.05 percent)
    - Nesosilicates:
        - Grossular, even a member of the garnet group (less than 1.54 weight percent)
        - Almandine (manganese contents less than 2.84 weight percent)
- Oxides
    - Hematite (manganese contaminations of maximum 1.87 wt % in clinopyroxene domained areas)
    - Magnetite (contaminations of manganese in braunite rich lamination less than 2.38 wt %)
    - Geothite (less than 1.11 weight percent)

- Carbonates
    - Strontian calcite, a variety of calcite (maximum of 1.45 weight percent manganese)
    - Calcite (contamination ranges from 0.79 up to 1.82 percent)
    - Dolomite (about 0.94 wt % manganese)

One of the most interesting minerals at Prabornaz is **piemontite**. Scanning electron microscope analyses gave values for wolfram about three percent. The origin of the wolfram is unknown, no wolfram minerals could be observed. These high percentages even can't be ignored and no other authors reported about wolfram in piemontite. At the beginning of my studies, I didn't pay that much attention at those high wolfram concentrations. In comparison with Tumanti et al. 2010 and Deer et al. 1997 any results for wolfram could be observed. Even intense literature research gave no results about the wolfram content in the piemontites.

The high amount of wolfram poses the question of the origin of wolfram, which can't be answered. Although wolframs character is partially siderophil and partially lithophil and its favorite occurrences are granites and sediments of basic to ultrabasic magmatites, any wolfram minerals can be detected. So the guesswork has be done, that wolfram and manganese were bedded in the same environment. Due to the processes of sedimentation primary wolfram and manganese minerals get formed. During the metamorphism the whole amount of wolfram minerals are changed to other minerals and the wolfram content became mobilized and attached in the piemontites. If this theory is true, the primary wolfram concentration was a multiple lesser than the primary manganese concentration.

Al_2O_3	17,80 - 18,61
SiO_2	35,92 - 37,63
K_2O	< 1,34
CaO	19,48 - 21,73
MnO	0,64 - 2,58
Mn_2O_3	13,24 - 18,49
FeO	2,16 - 2,91

Table 4-1: Variation of composition of Piemontite in weight percent (Oxides are given in mass%, ionic composition is calculated according to 12.5 oxygen atoms. Total content of MnO and Mn_2O_3 are calculated according to the method of Droop 1987)

Table 4-1 shows the variations of piemontite of all measured analyses. All measurements were done with the scanning electron microscope. In comparison with Deer et al 1997 the range of the different oxides is quite similar. But the comparison with Tumanti et al 2010 fits just with the upper limit of the measurements of this thesis. Although the manganese contents of Tumanti et al. 2010 correlates not at all. They've got values for MnO = 3.63 wt% and Mn_2O_3 = 12.81 wt%.

With a few piemontite analyses no calculation for Mn_2O_3 after Droop 1987 was possible, due to negative values for Mn_2O_3. Those values are plotted in table 4-2. The measured values for those piemontites, where no charge balance was necessary, fallow up with their values of aluminium, silicon and calcium at the upper limit of those values which are measured in table 4-1. As exception can be named iron, which shows smaller contents in those samples were no charge balance was possible, than those were a charge balance has to be done (compare table 4-1 and 4-2).

Al_2O_3	18,01 - 19,76
SiO_2	35,70 - 38,83
CaO	21,86 - 23,60
MnO	14,94 - 16,60
FeO	1,97 - 2,78
SrO	< 2,79
WO_3	< 2,30

Table 4-2: Variation of composition of those piemontites, where no charge balance was possible, in mass percent

Also very interesting observation could have been done. Rocks with a widespread of mineral composition are showing higher wolfram concentration than the monolithic sample SM39, where no wolfram can be detected.

I would recommend for doing some researches about the origin of the wolfram in this deposit. Furthermore wolfram couldn't be measured in any other mineral phase, then in those Epidotes. Maybe a relation to the manganese occurrences of the Ligurian orogeny can be found.

The main manganese ore of Prabornaz is formed by **braunite**, which have been measured in sample SM20, SM24 and SM35. The variations of their composition are printed in table 4-3.

SiO_2	9,29 - 10,27
MnO	3,57 - 8,19
Mn_2O_3	76,66 - 80,82
FeO	0,93 - 2,62

Table 4-3: Variation of composition of Braunite in weight percent (contaminations aren't plotted see table 3-1, table 3-7 or table 3-9) - (Oxides are given in mass%, ionic composition is calculated according to 12 oxygen atoms. Total content of MnO and Mn_2O_3 are calculated according to the method of Droop 1987)

Braunite analyses are unremarkable, although Tumanti et al 2010 MnO contents about 11.40 wt% and Mn_2O_3 contents with 76.86 recalculated. The measurements of table 3-7 show higher contents in Mn_2O_3 and lower contents in MnO in comparison to the values of Tumanti et al. 2010.

The Braunites of sample SM20 have been measured via Microprobe and those analyses produced the big amount of accessories, like sodium, aluminium, titanium, vanadium and chrome. Reason therefore is the different kind of analyzing system. By the microprobe analyses the wave dispersive system was chosen and the scanning electron microprobe analyses have been done with the energy dispersive system. Those measurements are a good example for the disadvantage of the energy dispersive system. Due to the fact, that the quantification limit isn't that high like that one of the wave dispersive system. The maximum of accessories (Na_2O, Al_2O_3, TiO_2, V_2O_3 and Cr_2O_3) has a total weight percentage of 0.244%, so those mass is irrelevant and both analyses systems can be compared together.

Analysis of sample SM20 (table 3-1) shows an irregularly high content of calcium with 3.5 wt%. Generally the calcium content stir in a range lower than 1 wt%. By deduction of this single analysis, the Braunit grain could have been found settled in an Augite. Probably the high calcium content results from the surrounding Pyroxene.

The ideal formula of Braunite is:

$$Mn^{2+} Mn_6^{3+} (SiO_4) O_8$$

Calculations of cations on the basis of 12 oxygen, in due considerations of charge balance from manganese, provides 0.31 to 0.68 cations Mn^{2+} and 5.97 to 6.11 cations Mn^{3+}. In comparison with Tumanti et al. 2010, the results on Mn^{3+} are a little bit higher than those and in contrast the Mn^{2+} results are a little bit lesser (Tumanti et al. 2010: $Mn^{3+} = 5.872$, $Mn^{2+} = 0.969$).

In samples SM20 have been alurgites analyzed, those analyses were done with the microprobe. The ideal formula of **alurgite** is:

$$K_2\,(Mg, Al)_{4\text{-}5}\,(Al, Si)_8\,O_{20}\,(OH)_4$$

The alurgite is a variety of muscovite. In sample SM48 a few muscovite minerals were analyzed with the scanning electron microscope. The ideal formula of muscovite is:

$$KAl_2\,(Al\,Si_3\,O_{10})\,(OH)_2$$

Due to no analyses of alurgites have been found in literature for comparison, table 4-4 should illustrate the differences of chemistry between muscovite and alurgite.

	Alurgite	**Muscovite**
Na_2O	0,00	0,49
MgO	7,42	3,09
Al_2O_3	15,59	27,74
SiO_2	53,26	51,82
SO_3	0,02	-
K_2O	9,26	11,02
CaO	0,00	-
TiO_2	0,41	-
V_2O_3	0,07	-
Cr_2O_3	0,00	-
MnO	1,99	-
FeO	1,26	3,04
ZnO	-	0,08

Table 4-4: Average d values of all measured alurgites and muscovites (values in mass percent)

A lot of different **garnets** have been analyzed. The main classification distinguished the garnets of this thesis in spessartine and almandine. Spessartines can be separated into two different varieties of spessartine (table 4-5). The first group has in his end members about 84.42 to 87.64 % spessartine, in the range of 4 percent almandine and more than 10 percent Grossular in his end member. The second group of spessartine rich garnets is characterized in his end members with three quarter of spessartine, one eighth of grossular, the other eighth is shared by almandine and pyrope, whereat pyrope just has an amount about one percent.

	Spessartine I	**Spessartine II**	**Spessartine III**
Almandine	< 5,73	4,83 - 8,48	15,96
Spessartine	84,42 - 87,45	77,56 - 77,94	73,00
Pyrope	< 0,53	1,11 - 11,12	8,39
Grossular	7,82 - 12,36	12,47 - 6,49	2,65

Table 4-5: Variation of different spessartine types (values in mass percent)

Also the almandines can be differenced into three kind of almandine (table 4-6). The first group is defined by about 90% almandine in his end member and about 10% pyrope, also a less content of grossular could be calculated (in the vary of two percent). The second group is represented by garnets with about 65% almandine and 22% pyrope, the rest is constant shared by spessartine and grossular.

	Almandine I	**Almandine II**	**Almandine III**
Almandine	82,23 - 90,67	78,52	64,24
Spessartine	< 0,05	1,21	6,59
Pyrope	7,31 - 11,47	15,13	6,23
Grossular	1,55 - 6,30	5,14	22,93

Table 4-6: Variation of different almandine types (values in mass percent)

In comparison with Tumanti et al. (2010) the results for the garnet composition are similar.

With the aid of the **fluid inclusions** minimum two different cycles of fluid migration can be observed. Due to the long alpine metamorphism history a big amount of inclusions could be observed, but most of them are too small for doing Raman measurements or microthermometry. The presents of CO_2 and N_2 could be demonstrated, but their amounts are to less for doing calculations about a percentaged composition. Ratios of the homogenizations temperatures and melting temperatures gave the hint of two different fluid cycles.

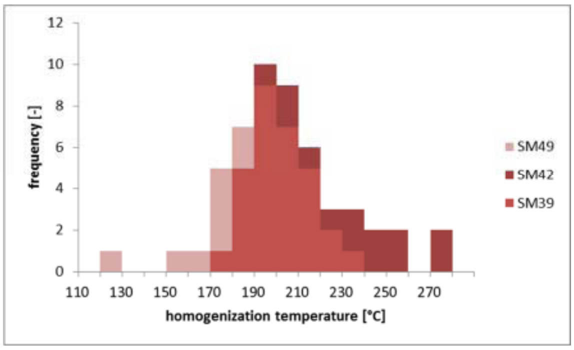

Diagram 4-1: Histogram of all measured homogenization temperatures (total values 52)

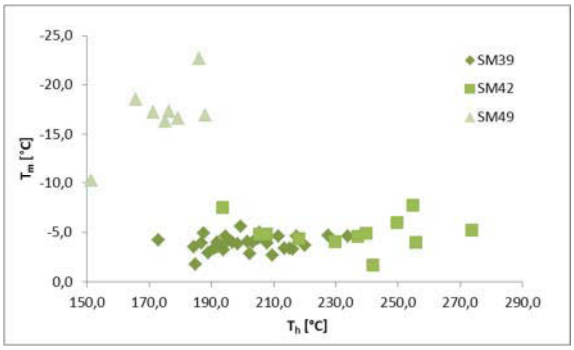

Diagram 4-3: Homogenization temperatures versus the melting temperatures of all measured fluid inclusions (total value 52)

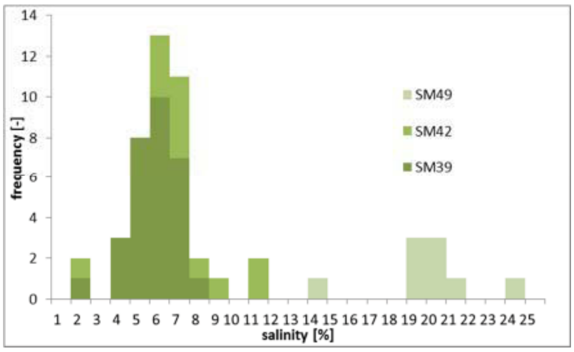

Diagram 4-2: Histogram of all measured salinities (total values 52)

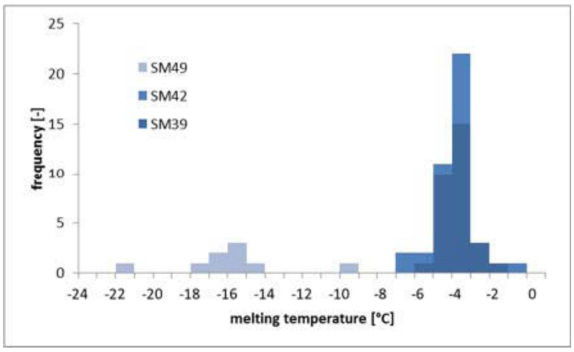

Diagram 4-4: Histogram of all measured melting temperatures (total values 52)

The homogenization temperatures of all fluid inclusion measurements together are forming a Gauss distribution over a range from 100°C (see diagram 4-1). These perfect distributions allow almost the interpretation of just one fluid phase process.

With a much more detailed look at the diagrams of the melting temperatures and salinity the guesswork of two different kinds of fluid phases is approvable. Diagrams 4-2 and 4-4 show a definitive trend of two different fluid phases. SM39, the Piemontite, correlates with SM42, the Garnet bomb, by their values of melting temperature and salinities. Both samples plotting in diagram 4-3 in the same range. Whereat the Garnet rich sample definitively much higher values for the homogenization temperatures is showing. The second fluid system is build up by SM49 with very high salinities, up to 20 %, in due to also very low melting temperatures. Even in diagram 4-4 they are plotting at a total different area, with lower homogenization temperatures and much lower melting temperatures. The guesswork of two different fluid phase systems can be done.

LIST OF REFERENCES

BAKKER, R.J. (2003): fluid package of computer programs for fluid inclusion studies, www.fluids.unileoben.ac.at

BEARTH, P. (1974): Zur Gliederung und Metamorphose der Ophiolithe Westalpen; Schweizerische mineralogische und petrographische Mitteilungen; Vol. 54; p. 385-397

DAL PIAZ, G. V.; BISTACCHI, A.; MASSIRONI, M. (2003): Geological outline of the Alps; Episodes; Vol. 26 no. 3; p. 175-180

DEER, W.A.; HOWIE, R.A.; ZUSSMAN, J. (2001): Rock forming Minerals, Vol. 4A Second Edition, framework Silicates: Silica Minerals, Feldspars; pp. 972

DEER, W.A.; HOWIE, R.A.; ZUSSMAN, J. (1997): Rock forming Minerals, Vol. 1B Second Edition, Disilicates and ring silicates; pp. 629

DIAMOND, L. (2001): Ore Deposits of Valle Saint Marcel

DROOP, G.T.R. (1987): A general equation for estimating Fe3+ concentrations in ferromagnesian silicates and oxides from microprobe analyses, using stoichiometric criteria; Mineralogical magazine 134; p. 549-552

GRIFFIN, W.L; MOTTANA, A. (1982): Crystal chemistry of clinopyroxenes from the St. Marcel manganese deposit, Val d’Aosta, Italy; American Mineralogist, Volume 67; Mineralogical Society of America; p. 568 – 586

EMSLEY, J. (2001): Nature’s building blocks: an A-Z guide to the elements; Oxford University Press; p. 249 – 253

FREY, M.; HUNZIKER, J.C.; FRANK, W.; BOCQUET, J.; DAL PIAZ, G.V.; JÄGER, E.; NIGGLI, E. (1974): Alpine metamorphism of the Alps: a review; Schweizer mineralogische und petrographische Mitteilungen; Volume 54; p. 247-290

HALL, D.L.; STERNER, S.M.; BODNAR, R.J. (1988): Freezing depression of NaCl-KCl-H_2O solutions; Economic Geology; Volume 83; p. 197-202

HILDEBRAND, H.J.; KIPPENBERGER, C.; KRAUß, U.; KRUSZONA, M.; SCHMIDT, H.; KAMPHAUSEN, D.; LIEBRUCKS, M.; RUMBERGER, M.; WETTING, E. (1977): VIII

Mangan, Untersuchungen über Angebot und Nachfrage mineralischer Rohstoffe; Bundesanstalt für Geowissenschaften und Rohstoffe; p. 156

MARTIN, S.; TAROTTI, P. (1989): Polyphase HP metamorphism in the ophiolitic glaucophanites of the lower St. Marcel Valley (Aosta, Italy); Ofioliti 14 (3); p. 135-156

MAYNARD, J.B. (1983): Geochemistry of sedimentary ore deposits; Chapter 5. Manganese; Springer-Verlag; p.121-145

PASSCHIER, C.W.; URAI, J.L.; VAN LOON, J.; WILLIAMS, P.F. (1981): Structural Geology of the central Sesia Lanzo Zone; Geologie en Mijnbouw 60; p.497-507

SCHMIDT, C.; ZIEMANN, M.A. (200): In-situ Raman spectroscopy of quartz: A pressure sensor for hydrothermal diamond-anvil cell experiments at elevated temperatures; American Mineralogist; Volume 85; p. 1725-1734

TAROTTI, P.; MARTIN, S.; POLINO, R. (1986): Geological data about the ophiolitic sequences in the St. Marcel Valley (Aosta Valley); Ofioliti 11(3); p. 343-346

TUMIATI, S.; MARTIN, S.; GODARD, G. (2010): Hydrothermal origin of manganese in the high-pressure ophiolite metasediments of Praborna ore deposit (Aosta Valley, Western Alps); European Journal of Mineralogy; 22; p. 577-594

WEISS, S.A. (1977): Manganese the other uses – A study of the Non-Steelmaking applications of Manganese; Metal Bulletin Books Ldt.; p. 360

ZHANG, Y.G.; FRANTZ, J.D. (1987): Determination of homogenization temperatures and densities of supercritical fluids in the system NaCl-KCl-$CaCl_2$-H_2O using synthetic fluid inclusions; Chemical Geology; Volume 64; p. 335—350